Experimental distinction between phase shifts and time delays: Implications for femtosecond spectroscopy and coherent control of chemical reactions

Allison W. Albrecht, John D. Hybl, Sarah M. Gallagher Faeder, and David M. Jonas

Citation: The Journal of Chemical Physics **111**, 10934 (1999); doi: 10.1063/1.480457
View online: http://dx.doi.org/10.1063/1.480457
View Table of Contents: http://scitation.aip.org/content/aip/journal/jcp/111/24?ver=pdfcov
Published by the AIP Publishing

Experimental distinction between phase shifts and time delays: Implications for femtosecond spectroscopy and coherent control of chemical reactions

Allison W. Albrecht, John D. Hybl, Sarah M. Gallagher Faeder, and David M. Jonas[a)]
Department of Chemistry and Biochemistry, University of Colorado at Boulder, Boulder, Colorado 80309-0215

(Received 19 May 1999; accepted 27 September 1999)

Two different definitions of phase shifts and time delays are contrasted and shown to match different experimental methods of generating delayed pulses. Phase shifts and time delays are usually defined in terms of a carrier wave in magnetic resonance, but definitions based on the envelope of a single pulse are useful in optics. It is demonstrated experimentally that a frequency domain measurement using spectral interferometry can simultaneously measure phase shifts with an accuracy of 0.1 rad (2σ) and time delays with a precision of 40 attoseconds (2σ) for 25 femtosecond optical pulses. Envelope time delays are generated by pathlength differences in an interferometer. Constant spectral phase shifts are demonstrated by diffracting pulses from a variable phase volume diffraction grating. Experimental requirements for phase-resolved spectroscopy are outlined. The theory of phase-locked pulse pair techniques is reexamined, and it is concluded that linear experiments with phase-locked pulse pairs are completely equivalent to Fourier transform absorption spectroscopy and do not measure the refractive index or real part of the susceptibility. It is shown that Fourier sine and cosine transformations of truncated time domain signals which do not match the symmetry of the complete signal can produce a false dispersive susceptibility because they are equivalent to Kramers–Kronig inversion of finite bandwidth absorption data. A procedure for shifting $\pi/2$ phase-locked transients by a quarter cycle of delay to generate a transient with a $\pi/2$ spectral phase shift is given. Equations used to calculate femtosecond nonlinear optical signals have assumed carrier wave delays. Modifications to these equations are required when envelope delays are generated by interferometer pathlength differences and modified equations are given. The modified equations yield significantly different results for phase-resolved or interferometric experiments. In particular, the modified equations are needed to calculate indirectly (interferometrically) detected frequencies and the real and imaginary parts of two-dimensional Fourier transform spectra. The role of the refractive index and real part of the frequency domain susceptibility in nonlinear experiments with phase-locked pulse pairs is explored. It is concluded that experiments such as the heterodyne detected stimulated photon echo are insensitive to nonlinear refractive index changes under some circumstances. Finally, modifications of some equations used in the theory of coherent control are needed to match theory with experimental practice. © *1999 American Institute of Physics.* [S0021-9606(99)00148-8]

I. INTRODUCTION

It has been recognized for several years that phase control is essential for the coherent control of chemical reactions by quantum mechanical interference effects[1–8] and also for some nonlinear optical experiments.[9–18] Although a distinction between phase shifts and time delays is made for radio frequency waves,[9,19] many excellent texts treat phase shifts and time delays as interchangeable in the optical region of the spectrum.[20–22] Common optical elements (e.g., waveplates, phase plates, compensators) often use one effect to approximate the other, which is possible because of experimental difficulties in measuring the difference. A distinction between phase shifts and time delays is readily appreciated for experimentally available femtosecond pulses consisting of only a few optical cycles (see Fig. 1).

Various distinctions between phase and delay have been made by workers in different fields. When pulses are generated by multiplying a carrier wave with time dependent envelopes, it is natural to define delay by the separation between the envelope maxima and define phase shift by extrapolating the carrier wave between pulses [e.g., $\exp[-(t-t_d)^2/\tau^2]\sin(\omega_0 t+\phi)$ where t_d is the delay, ω_0 is the carrier frequency, and ϕ is the phase-shift]. This ''carrier wave'' phase-shift is implicit in Ramsey's discussion of separated oscillatory fields[23] and elsewhere in magnetic resonance.[9] The advantage of this definition is that if one pulse excites dipoles which oscillate at the carrier frequency, the field oscillations of a second delayed carrier wave pulse will be phased to further excite the dipoles for every delay

a)Author to whom correspondence should be addressed. Electronic mail: david.jonas@colorado.edu

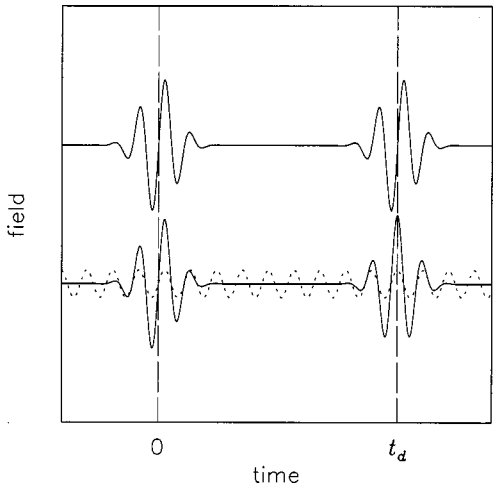

FIG. 1. Illustration of time domain distinctions between phase-shifts and time delays. The pulse envelopes have their maxima at the same time in both traces, hence the interpulse delay is the same in both traces. The top trace shows two delayed pulses generated by an ideal Mach–Zehnder interferometer with a variable delay line in one arm. These envelope delayed pulses are of the form $\exp[-(t-t_d)^2/\tau^2]\sin[\omega_0(t-t_d)]$ where t_d is the delay and ω_0 is the carrier frequency. For both pulses, the electric field passes through zero at the envelope maximum and reaches a maximum approximately half a cycle after the envelope maximum (i.e., the pulses are not phase-shifted in the envelope sense). The lower trace shows two pulses generated by multiplying a carrier wave $\sin(\omega_0 t)$ (dotted) with a delayed envelope, as generated by an ideal radiofrequency (RF) mixer. These carrier wave delayed pulses are of the form $\exp[-(t-t_d)^2/\tau^2]\sin(\omega_0 t)$ where t_d is the delay and ω_0 is the carrier frequency. If the carrier wave of the first pulse is extrapolated forward in time, it is in phase with the carrier wave of the second pulse (i.e., the pulses are not phase-shifted in the carrier wave sense). Note that the top trace, which has no phase-shift in the envelope sense, has a $\pi/2$ phase-shift in the carrier wave sense. In contrast, the lower trace is not phase-shifted in the carrier wave sense but exhibits a $\pi/2$ phase-shift in the envelope sense.

(unless the pulse or dipole is phase shifted). Carrier wave delays effectively shift the pulses into a ''rotating frame'' [24,25] so that the carrier frequency is aliased to zero independent of the sampling rate (i.e., the time domain transient oscillates only at difference frequencies $\pm(\omega-\omega_0)$ and not at the carrier frequency). The time domain reduction in sampling rate permitted by carrier wave delays is highly advantageous in magnetic resonance, where the fractional bandwidth $(\Delta\omega/\omega_0)$ of a spectrum is typically measured in parts per million. The price which must be paid for this reduction in sampling rate is a loss of information about whether an observed frequency lies above or below the carrier. Heterodyne detection, quadrature detection, and phase cycling are all used to restore this lost information in magnetic resonance.

In the optical region, Warren and Zewail showed that acousto-optic modulators could diffract nanosecond pulses with independently adjustable time delays and carrier wave phase-shifts from a continuous wave laser.[9] Warren and Zewail also experimentally observed oscillations in three pulse echo signals resulting from the simultaneous phase and delay variations produced by electro-optically sweeping the laser frequency into resonance with a molecular transition. The carrier wave pulse phase has been used in theoretical treatments of experiments using ''phase-locked pulse pairs,'' [11–14,16,18,26] nonlinear femtosecond spectroscopy,[27,28] and coherent control.[29–33] Hänsch and co-workers[34] used a different distinction between phase and delay in which the absolute phase is defined by comparing the maxima in the field oscillations to the maximum of the field envelope [e.g., $\exp[-(t-t_d)^2/\tau^2]\sin[\omega_0(t-t_d)+\phi]$ represents a pulse delayed by t_d and phase-shifted by ϕ]. At present, no method for measuring the absolute phase of an optical pulse has been demonstrated.[35] Hänsch and co-workers measured phase shifts between subsequent 8 fs pulses from a Ti:sapphire laser by interferometric cross-correlation and suggested that control over absolute ''pulse envelope'' phase might have applications in strong-field (nonperturbative) nonlinear optics.[34] With this definition, a delay is a time shift in the sense of the Fourier shift theorem,[36] which is advantageous in optical Fourier transform spectroscopy.[37,38] The advantages of systematic undersampling are greatly reduced in optical Fourier transform spectroscopy, where a fractional bandwidth of one-half is not uncommon.[37] In perturbative nonlinear optics, a distinction between phase and delay is relevant for experiments which are sensitive to the phase of the signal field through interference[16,18,39–43] and it is essential for theoretical calculations to match the experiment.

Without explicit statement, calculations of nonlinear optical signals[12–14,28,44,45] often exhibit various approximations which have been called ''quasimonochromatic.'' [46] For example, the approximate field $E(\vec{r},t)=e(t-t_d)\cos(\omega t-\vec{k}\cdot\vec{r})$ has a pulse envelope $e(t)$ that rises and falls simultaneously over all space, but field oscillations which propagate at the speed of light.[47] While the quasimonochromatic pulses have not been incorporated into essential aspects of the theory (which consider only a single point in space and usually use the coordinate dependence only symbolically), the picture of pulse propagation provided by quasimonochromatic approximations is misleading. The monograph by Schubert and Wilhelmi[48] treats time-domain nonlinear optics without quasimonochromatic approximations. Theoretical treatments of photon echo propagation[49,50] and the effect of impulsive stimulated Raman scattering on a single propagating femtosecond pulse[51,52] have incorporated traveling electromagnetic pulses and discuss how the spatially varying material response produced by one pulse interacts with subsequent traveling pulses. A reexamination of the slowly varying envelope approximation used to calculate nonlinear optical signals from the nonlinear polarization has shown that a closely related ''slowly evolving wave approximation'' is accurate for pulses consisting of a single cycle.[53] The name chosen by Brabec and Krausz emphasizes that a first order propagation equation (identical to that obtained from the slowly varying envelope approximation in one dimension) is valid if the *waveform* changes slowly during propagation over a wavelength.

The pulse envelope phase is a natural way to define phase shifts when the sample is larger than the wavelength of the radiation (as in far-field optical experiments), since an arbitrary electromagnetic plane wave propagates in vacuum without any change in the shape of the waveform.[54] For a plane wave propagating along the *z*-axis, the time-dependent electric field at any point in space can be obtained by substituting the retarded time, $t'=t-z/c$, into the time dependent

field $E(t)$ at the origin to account for the finite velocity of light. The retardation of a pulse without change in shape produced by a pathlength difference in vacuum (e.g., by adjusting one arm of a Mach–Zehnder interferometer) will be referred to here as a pure envelope delay. An advantage of this pulse envelope delay for optical experiments is that all molecules in a thin sample experience pulses with the same phase. In contrast, the relative carrier wave phase between noncollinear pulses differs across the sample. In dispersive media, the pulse envelope generally propagates at a group velocity which is different from the phase velocity of the field maxima and minima, shifting the phase of the field oscillations relative to the pulse envelope. This intuitive time domain definition of a phase-shift[34] is valuable but it will be shown that a closely related definition in terms of the frequency dependent spectral phase is advantageous for three reasons: (i) it allows phase-shifts to be defined for almost arbitrary pulses; (ii) it can be easily incorporated into standard nonlinear optical theory; (iii) it corresponds more closely to present experimental practice.

In this article, frequency domain measurements which distinguish phase-shifts and time delays for femtosecond pulses are demonstrated. The measurements use the technique of spectral interferometry,[55–57] which has been greatly improved through the introduction of a robust Fourier transform algorithm by Joffre and co-workers[58] and Fittinghoff *et al.*[59,60] Phase-shifted femtosecond pulses are experimentally generated. Definitions of phase-shifts and time delays which are compatible with nonlinear optical theory and experiments are presented. The information content of experiments with phase-locked pulse pairs is discussed. Equations for calculating nonlinear optical signals with pulses generated by an optical delay line are derived. The difference between these equations and those given by Mukamel and co-workers[28,61–65] (which uniformly assume carrier wave delays) is important for experiments which are sensitive to the pulse phase, but makes little difference otherwise. In some cases, the modified equations completely alter the interferometrically detected frequencies in two-dimensional Fourier transform spectroscopy because carrier wave delays alias the carrier frequency to zero while envelope delays do not. The equations given here have been used to calculate the real and imaginary parts of experimental two-dimensional Fourier transform optical spectra.[43,66,67] Previous articles have reported only absolute value 2D optical spectra.[45,64,68,69] The equivalence between frequency domain susceptibilities and time-domain impulse response functions in nonlinear spectroscopy is emphasized. The connection between absorption and dispersion and the imaginary and real parts of the susceptibility is discussed. The need to bring theoretical descriptions of femtosecond pulses into agreement with experimental practice in coherent control is emphasized.

II. THEORY

The definitions of phase-shifts and time delays given here differ from those usually used in optical spectroscopy. The definitions given here become particularly useful for pulses shorter than the homogeneous dephasing time (e.g., optical Bloch T_2) of the sample under study, since each molecule then interacts with the entire pulse and a phase-shift of the pulse can be distinguished from a time delay at a molecular level. These phase-shifts will be shown to play a simple role in the theory of resonant nonlinear optical experiments. The time-domain electric field $E(\vec{r},t)$ is a real-valued function which, in the absence of dispersion, can be written as

$$E(\vec{r},t)=e(t-\vec{k}\cdot\vec{r}/\omega)\cos[\phi(t-\vec{k}\cdot\vec{r}/\omega)], \tag{1}$$

where $e(t)$ is the pulse envelope, $\phi(t)$ is the temporal phase, and $\vec{k}$ is the wavevector. The $\vec{k}\cdot\vec{r}/\omega$ term represents retardation of a field propagating at the velocity of light in the medium (in vacuum, $\vec{k}\cdot\vec{r}/\omega=z/c$). A pulse with a linear time dependence of the temporal phase, $\phi(t)=\omega_0 t+\phi_0$, is said to be purely amplitude modulated.[9] The electric field in the frequency domain is defined by inverse Fourier transformation of $E(\vec{r},t)$ and is inherently complex-valued:

$$\hat{E}(\vec{r},\omega)=\int_{-\infty}^{+\infty}E(\vec{r},t)\exp(i\omega t)\,dt$$

$$=e(\omega)\exp[i\phi(\omega)+i\vec{k}\cdot\vec{r}], \tag{2}$$

where $e(\omega)$ is a real spectral envelope and $\phi(\omega)$ is the real spectral phase at the origin ($\vec{r}=0$). A pulse which is delayed by a time t_{delay} in the time domain [replacement of t by $(t-t_{\text{delay}})$ everywhere in $E(\vec{r},t)$] acquires an additional spectral phase which is proportional to the frequency: $\phi_{\text{delayed}}(\omega)=\phi(\omega)+\omega t_{\text{delay}}$ (Fourier shift theorem).[36] Since $\vec{k}$ is proportional to ω, the $\vec{k}\cdot\vec{r}$ term in Eq. (2) represents a spatially varying delay. Because $E(t)$ is real, $e(\omega)=e(-\omega)$ and $\phi(\omega)=-\phi(-\omega)+m2\pi$ (where m is any integer). Equation (2) has more generality than Eq. (1) because it is simple to incorporate material dispersion in $|\vec{k}(\omega)|=n(\omega)\omega/c$. Equation (2) has been used in a theoretical treatment of coherent control[70] and in a recent treatment of 2D THz spectroscopy.[71] Since $\hat{E}(\vec{k},\omega)=(2\pi)^3 e(\omega)\times\exp[i\phi(\omega)]\delta(\vec{k})$, the spectral phase, $\phi(\omega)$, is the easiest way to define phase in $\vec{k}$ space. Nonlinear optical signals can be separated in $\vec{k}$ space by macroscopic phase matching, so the spectral phase should be a particularly appropriate way to define phase in nonlinear optics. The power spectrum of the field,

$$I(\omega)\propto|\hat{E}(\omega)|^2=[e(\omega)]^2, \tag{3}$$

is completely independent of the spectral phase. If the power spectrum is known, then the spectral phase $\phi(\omega)$ uniquely determines $E(t)$. Unlike the spectral phase, a change in the temporal phase $\phi(t)$ can affect the frequency spectrum of the pulse as well as the spectral phase.[53] If a constant term in the temporal phase is adjusted, the time integral of the field changes for a sufficiently short pulse. The time integral of the field is the zero frequency Fourier component of the spectrum, so a temporal phase change can generate near zero frequencies. The generation of near zero frequencies requires a nonlinear process such as optical rectification[46] which is not present in the phase control mechanisms demonstrated to

date. Phase control mechanisms which do not generate new spectral components are usually most easily understood in the frequency domain.

To gain some insight into the connection between temporal and spectral phase, rotating wave decompositions of the frequency domain field are useful. Defining

$$\hat{E}_{\mathrm{rw}+}(\omega)\equiv(1/2)\int_{-\infty}^{+\infty}e(t)\exp[-i\phi(t)]\exp(i\omega t)dt,$$

and

$$\hat{E}_{\mathrm{rw}-}(\omega)\equiv(1/2)\int_{-\infty}^{+\infty}e(t)\exp[i\phi(t)]\exp(i\omega t)dt,$$

we have $\hat{E}(\omega)=\hat{E}_{rw-}(\omega)+\hat{E}_{\mathrm{rw}+}(\omega)$. Using this exact decomposition, addition of a constant ϕ_0 to the temporal phase $\phi(t)$ is equivalent to subtraction of ϕ_0 from the spectral phase $\phi_+(\omega)$ of $\hat{E}_{\mathrm{rw}+}(\omega)$ and addition of ϕ_0 to the spectral phase $\phi_-(\omega)$ of $\hat{E}_{rw-}(\omega)$. For positive ω, one can make a ''rotating wave'' approximation by retaining only half of the exact decomposition, $\hat{E}(\omega)\cong\hat{E}_{\mathrm{rw}+}(\omega)$, while for negative ω,$\hat{E}(\omega)\cong\hat{E}_{rw-}(\omega)$. Near $\omega=0$, the two rotating wave decompositions of $\hat{E}(\omega)$ can interfere so that the spectral phase is continuous on the circle 0, 2π [$\phi(\omega=0)$ can only equal 0 or $\pm\pi$ when $e(\omega=0)\neq 0$]. The two rotating wave approximations used above are applied only to the field. (In contrast, the rotating wave approximations used in calculating the resonant absorption of light are applied to both the field and the susceptibility.) So long as each rotating wave approximation has zero amplitude in the opposite range of frequencies, a constant temporal phase shift produces a constant spectral phase shift which abruptly changes sign at $\omega=0$. It is therefore sensible to define phase shifts by addition of a constant phase ϕ_0 to the spectral phase $\phi(\omega)$ for positive frequencies, so that $\phi(\omega)=\phi_0\,\mathrm{sign}(\omega)$; where $\mathrm{sign}(\omega)=+1$ for $\omega>0$, $\mathrm{sign}(0)=0$, and $\mathrm{sign}(\omega)=-1$ for $\omega<0$. Spano, Haner, and Warren have shown that the time-domain phase-shift of a pulse can be defined only for amplitude-modulated pulses without phase modulation.[10] *In contrast, the definition of a phase-shift as a constant spectral phase-shift allows an unambiguous definition of a phase-shift for any pulse whose spectrum does not extend to zero frequency.* It will be shown below (Sec. V) that this definition of a phase-shift allows extension of the phase cycling techniques used in magnetic resonance to chirped pulses (pulses with a nonzero temporal phase modulation $\partial^2\phi/\partial t^2$) in nonlinear optical experiments.

Spectral interferometry[55–58] determines the phase difference $\Delta\phi(\omega)$ between temporally separated signal and reference pulses by measuring the frequency domain interference fringes which result from spectrally resolving and hence temporally broadening the pulses so that they overlap in time. For infinite spectral resolution, the detected spectrum of the signal-reference pulse pair is given by

$$I(\omega)\propto|\hat{E}_{\mathrm{sig}}(\omega)+\hat{E}_{\mathrm{ref}}(\omega)|^2$$
$$\propto e_{\mathrm{sig}}^2(\omega)+e_{\mathrm{ref}}^2(\omega)+2e_{\mathrm{sig}}(\omega)e_{\mathrm{ref}}(\omega)\cos[\Delta\phi(\omega)]. \quad (4)$$

Provided the signal and reference spectra are known, Eq. (4) allows a unique (up to a sign) determination of the phase difference from the spectral interferogram. The sign of the spectral phase difference is uniquely determined if the sign of the delay between pulses is known. In order to fully resolve the interference fringes in the pulse pair spectrum, the pulse pair delay must be significantly less than the inverse of the spectrograph resolution.[12,42]

When material is added to the beam path, a pulse acquires an additional spectral phase $\phi(\omega)=(n(\omega)-1)l\omega/c$, where $n(\omega)$ is the index of refraction, l is the material length, and c is the speed of light. Regrouping the first two terms in the Taylor series expansion of the spectral phase into a constant term and a term which is linearly proportional to frequency yields[34]

$$\phi(\omega)=-\frac{l\omega_0^2}{c}\left.\frac{dn}{d\omega}\right|_{\omega_0}+\omega\frac{l}{c}\left[[n(\omega_0)-1]+\left.\frac{dn}{d\omega}\right|_{\omega_0}\omega_0\right]$$
$$+\frac{1}{2}\left.\frac{d^2\phi}{d\omega^2}\right|_{\omega_0}(\omega-\omega_0)^2+\cdots. \quad (5)$$

Note that the second- and higher-order terms have not been regrouped. The zero-order term is a phase shift resulting from the difference between phase and group velocity, the first-order term represents the extra material group delay, and higher-order terms represent pulse distortions (group velocity dispersion, etc.). If higher-order dispersion can be neglected, a graph of spectral phase as a function of frequency has the delay as slope and the phase shift as ϕ-intercept at $\omega=0$.

A constant phase-shift [$\phi(\omega)=\phi_0\,\mathrm{sign}(\omega)$] can be distinguished from the delay $t_d=\phi_0/\omega_{\mathrm{L}}$ [$\phi(\omega)=\omega\phi_0/\omega_{\mathrm{L}}$] which approximates that phase-shift near $\pm\omega_{\mathrm{L}}$ by measurement of the spectral phase $\phi(\omega)$ over a large bandwidth. At each frequency, the phase error $\delta\phi$ (in radians) is roughly the inverse of the signal-to-noise ratio of the fringes in the spectral interferogram.[72] A spectral interferogram with a shot noise limited signal-to-noise ratio of 256 [$(2^{16})^{1/2}$ assuming a 16 bit charge coupled device (CCD) camera] and a bandwidth of $\Delta\omega=0.10$ rad/fs (Gaussian transform limit 27 fs) should thus determine delays with an accuracy $\delta\phi/\Delta\omega\sim 40$ attoseconds. By extrapolating a linear spectral phase difference from $\omega\sim 2.3$ rad/fs back to zero frequency, constant phase shifts should be measured to within $\omega(\delta\phi/\Delta\omega)\sim 0.1$ rad. For reasons discussed in Sec. IV, the precision of the experimental results is slightly better than these simple estimates.

III. EXPERIMENT

Experiments used a variable repetition rate cavity dumped Kerr lens mode-locked Ti:sapphire laser and five beam interferometer described previously.[42] The five beam interferometer is constructed for passive stability but is not actively stabilized. Spectral interferograms were recorded using a spectrograph (SPEX 340S, 300 groove/mm grating) with a liquid nitrogen cooled CCD array (Princeton Instruments LN/CCD-1024E, 16 bit intensities) yielding 0.3 nm/pixel resolution on 1024 pixels. Spectra were corrected for pixel to pixel variations in sensitivity (which can affect the

recovered phase difference) but not for the slow variation of quantum efficiency with wavelength (which affects only the recovered spectrum and not the recovered phase differences). Without moving the spectrometer grating, CCD spectra were calibrated with 6–10 unblended atomic emission lines from an argon lamp (Oriel model 6030) and fit to an evenly spaced wavelength/pixel axis with a standard deviation of ~0.04–0.07 nm. (After this article was submitted, an article by Dorrer[73] demonstrated that spectrometer calibration errors can be important in spectral interferometry. Subsequent investigation revealed that a shift of up to 0.3 nm (1 pixel) between the calibration spectrum and interferogram may have occurred through misalignment of the lamp.) Integration times were 10 ms for time delays (100 kHz repetition rate) and 1 s for phase shifts (10 kHz repetition rate). The observed interference fringe depths were greater than 90% of the maximum possible $(I_{\max}-I_{\min})$ fringe depth of $4(I_{\mathrm{ref}}I_{\mathrm{sig}})^{1/2}$. The reference pulse typically arrived at the beamsplitter ~700 fs before the signal. This delay reduces the maximum possible fringe depth by 4%.[42] Spectral interferograms were recorded before and after the signal was altered, and the difference between spectral phases recovered from two spectral interferograms was used to cancel the spectral phase of the reference pulse and detect only the change in spectral phase of the signal.

Delays were generated by a stepper motor translation stage (Newport UTM100PP.1) with a nominal stepsize of 100 nm (0.66 fs delay). Constant phase shifts were generated by scattering a pulse off a variable phase volume diffraction grating. The variable phase diffraction grating was generated by adjusting the delay between two temporally overlapping noncollinear pulses (4.6° crossing angle) which excited a transient grating in a homogeneously broadened absorbing sample.[43] The pulse duration was 29 fs, the pulse energy was 270 pJ/pulse, and the focused beam diameter was 40 μm. To produce a pure population grating, electronic dephasing must be complete before the diffracted pulse arrives at the sample.[44,74] The sample was a room temperature 0.4 mM solution of the dye IR 144 in methanol flowing through a 0.1 mm path length cell at 1–2 m/s. In methanol, IR 144 exhibits complete electronic dephasing in tens of picoseconds and has no static inhomogeneous broadening.[75] The third pulse (*c*) arrived at the sample 100 ps after the two approximately coincident pulses (*a* and *b*) which created the grating, and the diffracted pulse with wave-vector $\boldsymbol{k}_{\mathbf{c}}+\boldsymbol{k}_{\mathbf{b}}-\boldsymbol{k}_{\mathbf{a}}$ was overlapped with a delayed reference pulse at a beamsplitter and characterized by spectral interferometry.[42] The effect of a fused silica plate was investigated by collecting interferograms with the signal beam passing through a tilted fused silica plate before recombination with the reference. The signal delay was adjusted to bring the two pulses within the inverse spectrograph resolution and obtain acceptable fringe depth. The 1.58 mm plate was tilted from 0° to 23.5° to produce a 2π phase-shift over the bandwidth of the laser.

IV. DATA ANALYSIS

A variant of a well-studied complex Fourier algorithm[58,76,77] was used to recover the amplitude and the phase of the signal from the spectral interferograms.[42] The algorithm consists of: (i) multiplication by the Jacobian $(1/\lambda)^2$ to transform the interferogram from an evenly spaced wavelength axis onto an unevenly spaced frequency axis; (ii) inverse Fourier transformation of the spectral interferogram into the time domain; (iii) filtering away the envelopes near $t=t_{\mathrm{ref}}-t_{\mathrm{signal}}$ and $t=0$ while retaining only the interference term near $t=t_{\mathrm{signal}}-t_{\mathrm{ref}}$ (this also removes much of the noise);[72] (iv) Fourier transformation to recover the product of complex fields $\hat{E}_{\mathrm{signal}}(\omega)\hat{E}^{*}_{\mathrm{ref}}(\omega)=e_{\mathrm{signal}}(\omega)e_{\mathrm{ref}}(\omega)\times\exp[i\Delta\phi_{sr}(\omega)]$; (v) recovery of $\Delta\phi_{sr}(\omega)=\phi_{\mathrm{signal}}-\phi_{\mathrm{ref}}$ over the range $[0, 2\pi)$ and unwrapping to remove discontinuities. Unwrapping proceeds outward from the center of the spectrum to avoid random 2π jumps from phase noise at the edge of the spectrum. Since accurate interpolation of the oscillatory interferogram from an evenly spaced wavelength axis to an evenly spaced frequency axis is difficult, both Fourier transforms are actually implemented as fast Fourier transforms between the uneven frequency axis and ''quasi-time.'' In all cases, the difference between spectral phases recovered from two spectral interferograms was used to cancel the spectral phase of the reference and obtain the change in spectral phase of the signal. Linear least-squares fitting of these spectral phase differences over the full width at half maximum of the pulse spectral envelope $e(\omega)$ recovered the delay as slope and the phase shift as the $\omega=0$ intercept. Since multiples of 2π are not physically significant, multiples of 2π have been added to the experimental phase differences to make comparisons with theory.

The effect of noise on the phase shift and time delay recovered from a spectral interferogram was investigated using simulated 16 bit data which included both Poisson distributed shot noise and Gaussian distributed CCD read noise (5 counts rms) on each pixel. The limiting accuracy was found to be about 8 attoseconds for time delays and 0.02 rad for phase shifts. Twenty repeated experimental reference-signal phase differences recorded at a fixed delay yielded least-squares fit standard errors of 0.018 rad in the spectral phase, rms differences of 0.06 rad in the phase shift, and a standard deviation of 22 attoseconds in the delay between successive interferograms. The standard errors of repeated measurements agree with the typical 1σ linear least-squares fit estimates of the phase-shift error (0.05 rad) and delay error (20 as) recovered from single interferograms.

Changes in delay between two pulses were generated by moving the delay stage of the signal beam over a range of 400 fs while collecting spectral interferograms between the reference and signal. Figure 2 shows the first few experimental (0–4 fs) spectral phase differences recovered from this series of time delayed spectral interferograms along with linear least-squares fits to the data. The fit lines are extrapolated to zero frequency to demonstrate the accuracy of the $\omega=0$ intercepts $(2\sigma=0.1\,\mathrm{rad})$, which are not constrained in the least-squares fit. The zero intercepts indicate there are no constant spectral phase shifts as the pulse delay is varied, as expected for an optical delay line from Maxwell's equations. In contrast, the change in the spectral phase of a carrier wave pulse with delay t_d is $\Delta\phi(\omega)=(\omega-\omega_0)\,t_d$ so that the spectral phase of a carrier-wave delayed pulse would remain zero at the carrier frequency ω_0 while the ϕ-intercept would vary

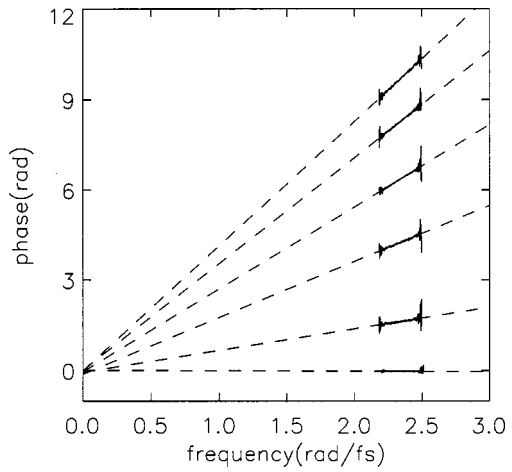

FIG. 2. Spectral phase differences recovered from a series of time delayed spectral interferograms. The dashed lines are linear least-squares fits to the experimental data shown as solid lines over the frequency range 2.2–2.5 rad/fs. The dashed lines are extrapolated to zero frequency to demonstrate the accuracy of the intercepts, which are not constrained in the least-squares fit. The zero intercepts indicate there are no constant spectral phase shifts as the pulse delay is varied. The precision of the measurements was determined from the standard deviations of the phase and delay recovered from a series of consecutive interferograms recorded with no change in delay. The typical standard error of the linear least-squares spectral phase fit was 0.018 rad, the delay precision was 20 attoseconds (1σ), and zero intercepts were correct to 0.05 rad (1σ). The delays (from bottom to top) are: 0.01, 0.71, 1.86, 2.73, 3.53, and 4.14 fs. The zero delay spectral phase was obtained by subtracting two consecutive spectral phase differences without moving the delay line. The variation of the experimental phase differences at the lowest and highest frequencies shown results from the low signal amplitude at these frequencies.

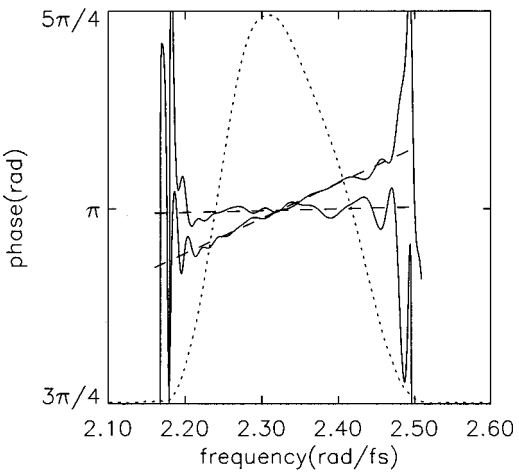

FIG. 3. Distinction between a phase-shift of π and a half-cycle of delay in the spectral phase. The recovered electric field envelope $e(\omega)$ is shown as a dotted line. The experimental phase differences $\Delta\phi(\omega)$ are shown as solid lines. Dashed lines show unconstrained linear least-squares fits to the spectral phase over the full width at half maximum of the field envelope. The spectral phase is well determined over the center of the envelope but starts to oscillate as the amplitude vanishes. The smooth waves in the spectral phase are a result of the time domain filtering in the Fourier algorithm. The nearly horizontal phase difference corresponds to an approximate π phase shift with best fit line $\phi(\omega)=\omega(\text{rad/fs})\times 0.072(26)\ \text{fs}+2.967(59)$ rad. The diagonal phase difference corresponds to a time delay of approximately half an optical cycle with a line of best fit given by $\phi(\omega)=\omega(\text{rad/fs})\times 1.406(14)\ \text{fs}-0.133(31)$ rad. 1σ error estimates from the linear least-squares fit are given in parentheses (in units of the last specified digit). Near 800 nm (optical period 2.67 fs), 41 nm bandwidth pulses (transform limit $\sim$23 fs) are sufficient to establish a clear experimental distinction between a phase-shift and a time delay.

as $-\omega_0 t_d$. When the time delay was decreased from 800 to 400 fs, the above algorithm recovered a systematic change in the average phase shift of -0.4 rad (i.e., the average phase at $\omega=0$ was 0 at 800 fs delay and -0.4 rad at 400 fs delay). The origin of this delay dependent phase-shift is not known [only a 0.003 rad shift is predicted for a 1.2×10^{-4} m path in air by Eq. (5)]. The simplest explanation (suggested by Dorrer's work)[73] is a constant 0.4 rad/400 fs (0.33 nm at 800 nm) frequency calibration error, but it might also arise from either inadequate automated filter positioning in the Fourier algorithm (filtering shifts of the time domain pulse envelope by 0.17 fs would generate a 0.4 rad phase error) or the frequency and delay dependent reduction in interferogram fringe amplitude caused by finite spectrograph resolution.[42] A constant frequency error could account for the observed 0.4 rad phase shift with 400 fs delay as a mislocation of the frequency origin.

Phase shifts were generated using interferograms collected from transient grating signals when the third (scattering) pulse was delayed by 100 ps. Adjusting the delay between the first two pulses through one optical period adjusts the phase of the volume diffraction grating they excite through 2π.[43] This change in grating phase is directly transferred to the phase of the diffracted signal.[78] The spectral phase differences recovered from interferograms for a π phase-shift and a half cycle delay (1.33 fs delay) are contrasted in Fig. 3. The signal to noise of the interferograms used to recover the π phase-shift in Fig. 3 is lower than that of the delay interferograms used here and for Fig. 2. The phase-shift and time delay were determined from unconstrained fits to the spectral phase over the full width at half maximum of the field envelope $e(\omega)$. The differences in phase-shift and time delay between the π phase-shift and half cycle delay both exceed 40 sample deviations. The constant spectral phase-shift of the signal shown in Fig. 3 is not predicted by calculating the nonlinear optical signal assuming carrier wave delayed excitation pulses, but is reproduced when envelope delays are used (Sec. V C).

V. DISCUSSION

We have shown experimentally that phase-shifts and time delays can be separately measured and defined in terms of their effect on the spectral phase. Most theoretical treatments of the nonlinear field–matter interactions underlying femtosecond spectroscopy and coherent control experiments have employed quasimonochromatic approximations and used time delays defined in the carrier wave sense. A careful distinction between phase and delay requires changes in the practical implementation and theoretical calculation of experiments which measure or exploit electronic interference. We first discuss experimental requirements for a phase-sensitive optical experiment. Since many experiments in nonlinear optics[16,18,79–81] and coherent control[82–85] use phase-locked pulse pairs, we then clarify the material properties measured with linear phase-locked pulse pair spectros-

copy before discussing nonlinear spectroscopy. A time-domain distinction between ''heterotime'' and ''homotime'' techniques which is analogous to the distinction between frequency domain heterodyne and homodyne techniques[86] and directly relates to measured material properties is proposed. Finally, we discuss coherent laser control of chemical reactions.

A. Experimental practice

Zero-order wave plates have been used to introduce phase shifts[58,87] and found to produce unwanted time delays when they are used to rotate polarization.[88] The phase-shift and delay between the *e* and *o* rays produced by an 800 nm zero-order half-wave plate were calculated from the refractive indices for crystalline quartz.[89] (The calculation was checked by comparing to previously measured phase and group velocities for fused silica[90] and carbon disulfide.)[91] At 800 nm, the waveplate introduces a phase shift between the ordinary and extraordinary rays of $+0.191$ rad and a delay of -1.415 fs [i.e., the ordinary ray arrives before the extraordinary so that $(\phi_o+\omega t_o)-(\phi_e+\omega t_e)=-\pi$]. A delay of *more* than half an optical cycle is thus compensated by a constant phase shift to produce an $e-o$ phase difference of π at 800 nm. The group velocity dispersion difference between the two rays is 0.08 fs^2, which is completely negligible for most pulses.

Tilted glass plates have been used to introduce either phase shifts[87,92] or time delays[93] which is possible for narrow band pulses when the two are practically indistinguishable. We investigated whether tilting a fused silica plate could be used to introduce constant spectral phase-shifts for broadband pulses if the delay were adjusted for. We found that tilting a 1.58 mm fused silica plate from normal incidence to 23.5° incidence produced a 1 rad phase nonlinearity over a 39 nm bandpass while it was calculated to produce 0.5 rad nonlinearity. Although the reason for this discrepancy is not known, we conclude that small angular adjusts of fused silica plates (e.g., beamsplitters) do not significantly change the phase and that the large angular adjusts required to change the phase are not useful because of higher-order dispersion. A further implication concerns tolerances for optical thickness, which are usually specified to minimize differences in group velocity dispersion [second-order term in Eq. (5)]. For phase-resolved femtosecond experiments, thickness tolerances must be more tightly specified to minimize constant phase differences [zero-order term in Eq. (5)]. For fused silica at 800 nm, a 0.5 μm thickness difference in a 45° beamsplitter adds a nearly constant spectral phase of 0.1 rad.

Reflection off a dielectric mirror or beamsplitter can produce no phase-shift, a pure π phase-shift, or a frequency dependent phase-shift.[21,94] If two pulses generated by a lossless beamsplitter are recombined at an identical beamsplitter, the spectral phase differences in the two output arms of the second beamsplitter must differ by a frequency independent π phase-shift in order to conserve the total spectrum (the fringe patterns observed in the spectral interferograms of the two output arms of the interferometer must add up to the input pulse spectrum). The number and type of reflections must therefore be equal for all beams to avoid unwanted π phase shifts (e.g., for white light, an ideal Michelson interferometer usually has a dark fringe at zero delay[20,22] while an ideal Mach–Zehnder interferometer has a white fringe at zero delay).[22] A Mach–Zehnder interferometer has been found necessary to produce correct interferometric autocorrelations for sub-10 fs pulses.[95]

Bragg diffraction off a volume grating causes a wavelength dependent angular dispersion,[20] but this angular dispersion can be practically negligible when the grating spacing is large (e.g., a 15 μm grating spacing in an acousto-optic cavity dumper caused negligible angular dispersion for 13 fs pulses).[96] If the phase of the volume grating is shifted by translating all the maxima and minima along the grating wavevector while keeping the grating envelope fixed, the grating phase-shift is directly translated into a frequency independent phase-shift of the diffracted beam[78] as demonstrated here in Fig. 3. This transfer of grating phase shifts to the diffracted pulse is used in cavity-dumping mode-locked lasers[19] and is the basis for controlling the phase difference between pulses using acousto-optic diffraction.[9] A third method for producing pure spectral phase shifts is to spectrally disperse the pulse and phase-shift individual frequency components with the phase masks used by Nelson, Weiner, and co-workers[97] or the extended acousto-optic modulators used by Warren and co-workers.[98] Careful investigation has revealed that these methods couple time delay and lateral beam position.[99]

B. Phase-locked pulse pairs

Femtosecond phase-locked pulse pairs[11–13,16,18,79–83] are used in nonlinear spectroscopy and coherent control. In optical spectroscopy, phase-locked pulse pairs have been obtained by two distinct classes of experimental methods. The first method proposed by Salour and Cohen-Tannoudji,[100,101] but not implemented until later by Warren and Zewail,[9] uses amplitude modulation of a continuous wave train to produce pulses which have no carrier wave phase-shift when either delay or frequency is adjusted. Substituting the spectral phase-shift between carrier wave delayed pulses, $\Delta\phi=(\omega-\omega_0)t_d$, into Eq. (4) shows that the spectrum of the pulse pair always has a maximum at the carrier frequency ω_0. This constant intensity at the carrier frequency makes carrier wave delays particularly suitable for optical Ramsey-fringe spectroscopy.[23,100–102] The second method proposed by Salour and Cohen-Tannoudji uses an interferometer to generate the pulse pair and actively stabilizes the path length difference with a reference beam.[10,100,101,103] In the second method, there is no envelope phase-shift as the delay is adjusted, but by using the cw carrier wave as a reference and actively stabilizing the optical path difference to an integral number of carrier wavelengths, one can select only those envelope delays which have no carrier wave phase-shift.[100,101] This technique has come to be known as ''phase-locking'' because it locks the carrier wave phase onto zero as the delay is discontinuously varied. Fourkas *et al.*[103] used a reference interferometer to stabilize and scan the relative carrier wave phase difference between temporally nonoverlapping picosecond pulses, but the phase difference between pulses could not be determined by this method.

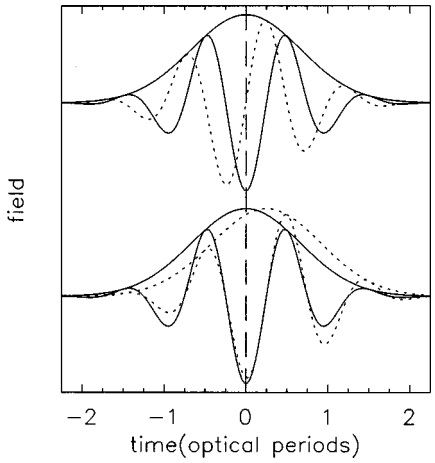

FIG. 4. Calculated difference between a reference pulse, a pulse with a $\pi/2$ spectral phase-shift, and a pulse with a quarter cycle of delay in the time domain. The top two traces show a pair of pulses with a $\pi/2$ spectral phase-shift. The dotted line shows the reference pulse and the solid line shows the $\pi/2$ phase-shifted pulse. The envelopes of the two pulses are almost exactly the same and only the solid envelope is visible. The bottom two traces contrast a $\pi/2$ phase-shifted pulse (solid) with a $\pi/2$ phase-locked pulse (dotted). The $\pi/2$ phase-locked pulse has a quarter-cycle envelope delay relative to the reference pulse in the top part of the panel. The two pulse envelopes on the lower traces are visibly different, but both fields oscillate through zero at the same points. Both pulses in the lower trace have the desired carrier wave phase-shift relative to the reference, but phase-locking approximates the desired delay. In contrast, from an envelope delay view, only the envelope delay differs between the dotted traces and the dotted traces are not phase-shifted relative to each other (the constant term in the spectral phase is the same).

Scherer *et al.*[11–13] introduced a powerful and more general experimental method for phase-stabilizing temporally separated femtosecond pulses by broadening the pulses in a monochromator and using interference fringes at a single wavelength (the locked wavelength) to actively stabilize the pathlength difference to a set number of quarter-wavelengths. More precisely, feedback adjustments of a delay line achieve and maintain spectral phase differences of 0, $\pi/2$, π, or $3\pi/2$ at the locked wavelength (this spectral phase difference includes both any interferometer imperfections and the delay). Lock-in amplifiers which detect high harmonics of spectrally resolved interference fringes between delayed pulses have been used to phase-lock on smaller fractions of 2π as a method for actively stabilizing envelope delay.[79,81–83]

In order to maintain a constant spectral phase difference of ϕ at the locked frequency ω_{L} in a phase-locked experiment, the envelope delay between pulses is restricted to the discrete set of values $t_d=(2\pi n+\phi)/\omega_{\mathrm{L}}$, where n is an integer [Eq. (2.2) of Ref. 12 with error $\delta n=0$]. Calculated time domain differences between a reference pulse, a pulse with a constant $\pi/2$ spectral phase shift, and a $\pi/2$ phase-locked pulse are illustrated in Fig. 4. Substituting $(t-t_d)$ for t in Eq. (1), the above restriction on the envelope delay can be interpreted in two ways. From the envelope delay view, phase-locking with a nonzero phase-shift uses an extra envelope delay $\delta t=\phi/\omega_{\mathrm{L}}$ generated by a Mach–Zehnder interferometer to approximate the desired constant spectral phase shift ϕ near the locked frequency but does not alter or control constant differences in the spectral phase.[104] Alternatively, from a carrier wave viewpoint, setting the locked frequency to the carrier frequency and phase-locking reproduces the desired carrier wave phase-shift exactly $[\omega_0(t-t_d)=\omega_0 t-\phi]$, but changes the pulse delay. This carrier wave view of phase-locking was presented in the articles by Scherer *et al.*,[12,13] but their analysis makes it clear that it is desirable to record $\phi=0$ and $\phi=\pi/2$ transients at the same delay.

The analysis of these experiments[13] used delayed pulses generated by amplitude modulation with a controlled carrier wave phase-shift (appropriate to the first class of experiments proposed by Salour and Cohen-Tannoudji). Methods for handling the quarter-cycle change in interpulse delays between the $\phi=0$ and $\phi=\pi/2$ transients were not explicitly discussed.[105] It was claimed that measurements of excited state population as a function of delay for phase-locked pulse pairs with relative phases of 0 and $\pi/2$ completely characterize the optical free induction decay and directly determine both the real (dispersive) and imaginary (absorptive) parts of the linear susceptibility within the range of the pulse spectrum without Kramers–Kronig inversion.[12] A free induction decay includes radiation from superposition states which involve both resonantly excited transitions (dipole phase $\pm\pi/2$ with respect to excitation field giving rise to absorption or stimulated emission) and nonresonant, virtually excited transitions with Bohr frequencies which may lie either inside or outside the pulse spectrum (dipole phase 0 or π with respect to excitation field giving rise to dispersion and the refractive index). A second article stated more precisely that phase-locked pulse pair experiments completely determine the complex linear susceptibility within the pulse spectrum arising from transitions within the pulse spectrum.[13] This last qualification is puzzling because the result resembles a calculation of the dispersive susceptibility based on finite bandwidth absorption data, but such a calculation should be equivalent to a Kramers–Kronig inversion.

Using a carrier-wave phase, Heller emphasized the close relationship of linear phase-locked experiments which detect total excited state population to continuous wave absorption spectroscopy.[106] Bavli *et al.*[107] used a carrier wave phase and noted that restricted $(0,\infty)$ Fourier transforms of the $\phi=0$ and $\phi=\pi/2$ interference signals could be combined to resemble the absorption coefficient and refractive index in the region of anomalous dispersion. Warren *et al.* suggested that the femtosecond phase-locked pulse pair experiments were the first demonstration of true optical Fourier transform spectroscopy.[4] Later calculations on Rydberg wave packets used path length delayed pulses (with no envelope phase shift) and concluded that the linear time domain phase-locked signal was determined by the Fourier transform of the product (absorption cross section)×(pulse spectrum).[108,109] Blanchet *et al.*[110] have noted that linear spectroscopic experiments with path length delayed femtosecond pulse pairs are completely equivalent to Fourier transform spectroscopy. These conclusions thus apply to the original phase-locked pulse pair experiments on molecular I_2.[11–13]

When the sample is outside the interferometer (either before or after), Fourier transform (FT) spectroscopy mea-

sures the absorption spectrum and is not sensitive to the refractive index (power FT spectroscopy).[37] When the sample is before or after the interferometer, the refractive index of the sample produces the same spectral phase change in each beam. The two identical phase changes cancel and are not converted into an observable amplitude change of the recombined beams. The key to measuring refractive indices is converting a phase shift of only one beam into an amplitude change of the recombined beams.[21] Optical Fourier transform spectroscopy can measure refractive index differences if the sample is placed in only one arm of the interferometer (amplitude FT spectroscopy[37] or dispersive FT spectroscopy[111]). In magnetic resonance, direct detection of a free induction decay by heterodyne or quadrature methods which combine a causally generated signal with a local oscillator outside the sample is analogous to placing the sample in one arm of an optical interferometer and actually measures both the absorptive and dispersive parts of the magnetic susceptibility.[112] In contrast to the phase-locked pulse pair experiments (where the sample is outside the interferometer), amplitude FT measurements detect contributions to the refractive index from absorption transitions outside the spectrum of the pulse. The theory of FT spectroscopy thus shows the linear phase-locked pulse pair experiment of Ref. 13 measured only the absorption coefficient because the pulses were not phase-shifted in the envelope sense. The question of whether separate phase and delay control would allow measurement of both refractive index and absorption coefficient (hence real and imaginary susceptibility) is important for nonlinear optical experiments which use phase-locked pulse pairs and will be reexamined below.

Before quantum mechanical analysis, we give a suggestive frequency domain argument. A single time domain data point in a fluorescence detected phase locked pulse pair transient can be understood as one data point in the Fourier transform of the product $\sigma_{\mathrm{fl}}(\omega)I(\omega)$ (fluorescence excitation spectrum$\times$pulse spectrum). Pulse pair spectra are consinusoidally modulated $I(\omega)[1+\cos(\omega t+\phi)]$ where t is the delay between pulses in the pair, $I(\omega)$ is the single pulse spectrum, and ϕ is the constant spectral phase-shift between pulses. At each frequency (linear response), the fluorescence excited by the pulse pair is proportional to the product $\sigma_{\mathrm{fl}}(\omega)I(\omega)[1+\cos(\omega t+\phi)]$. The photomultiplier measures the frequency integral of this quantity. A lock-in subtracts the integral of $\sigma_{\mathrm{fl}}(\omega)I(\omega)$ (single pulse contributions) and returns the frequency integral of the two pulse interference term $\sigma_{\mathrm{fl}}(\omega)I(\omega)\cos(\omega t+\phi)$. At each pulse pair delay t, the output of the lock-in is the Fourier transform (cosine transform for $\phi=0$) of the product $\sigma_{\mathrm{fl}}(\omega)I(\omega)$ evaluated at the time t. The spectral phase shift ϕ controls how the time domain experiment Fourier transforms the product $\sigma_{\mathrm{fl}}(\omega)I(\omega)$. The analysis below shows that even with arbitrary phase control, linear phase-locked experiments can be completely predicted from the linear absorption spectrum within the bandwidth of the excitation pulses and are insensitive to the refractive index. A purely time domain analysis also leads to the conclusion that dispersive components of the susceptibility are not detected if each pulse is treated both as a polarization excitation source and as an interference field for radiation emitted by the polarization excited by the other pulse. The articles by Scherer *et al.*[12,13] noted similarities between phase-locking and systematic undersampling in optical Fourier transform spectroscopy. It will be demonstrated that linear phase-locked experiments are completely equivalent to systematically undersampled Fourier transform spectroscopy[38] with femtosecond pulses, where phase-shifts are needed to recover the absorption spectrum. A fast Fourier transform procedure for correcting interferometer imperfections and shifting phase-locked transients by a quarter-cycle delay will be given.

The starting point for our discussion of linear phase-locked pulse pair experiments with constant spectral phase shifts is the first-order time dependent perturbation theory result for the transition probability.[113] Following the treatment in Ref. 13, all dephasing processes will be assumed slow and neglected. After excitation by a weak, brief pulse of light, the transition probability P_{ij} from ground state i to excited state j is given by $P_{ij}=|\mu_{ji}\cdot\hat{E}(\omega_{ji})/\hbar|^2$ where μ_{ji} is the transition dipole matrix element, ω_{ji} is the Bohr transition frequency $(E_j-E_i)/\hbar$, $\hat{E}(\omega)$ is the Fourier transform of the pulse electric field, and $\hbar$ is the reduced Planck constant. When the spectrum of the pulse pair [Eq. (4)] is substituted in the transition probability, one obtains

$$P_{ij}=2|\mu_{ji}/\hbar|^2|e(\omega_{ji})|^2(1+\cos[\Delta\phi(\omega_{ji})]). \tag{6}$$

The transition probability for linear absorption of a pulse pair depends on the spectral phase difference between the pulses, but is independent of the actual phase structure of the separate pulses. This result is also valid for incoherent (white) light,[114] thus establishing a complete equivalence with Fourier transform spectroscopy if the power of the transmitted train of pulse pairs is measured as a function of delay. For delayed pulses with a varying frequency domain phase-shift, the spectral phase difference can be written as $\Delta\phi(\omega)=\omega t_d+\phi_0(\omega)$ where $\phi_0(\omega)$ is the spectral phase difference between pulses at zero delay. The choice of $t_d=0$ is unavoidably somewhat arbitrary when $\Delta\phi(\omega)$ is not a linear function of frequency because the group delay $d\Delta\phi/d\omega$ cannot be set to zero at all frequencies simultaneously. For delayed pulses with a constant spectral phase-shift, the spectral phase difference is given by $\Delta\phi(\omega)=\omega t_d+\phi\,\mathrm{sign}(\omega)$ and there is no ambiguity about zero delay. Assuming zero initial excited state population, the population interference signal detected in a linear phase-locked pulse pair experiment is

$$P^{\mathrm{int}}(t_d)=\sum_{i<j}2VN_i|\mu_{ji}e(\omega_{ji})/\hbar|^2\cos[\omega_{ji}t_d+\phi_0(\omega_{ji})], \tag{7}$$

where N_i is the number density of molecules in state i and V is the detection volume. If the envelope delay spectral phase in Eq. (7) is replaced by the carrier wave spectral phase $\phi(\omega)=(\omega-\omega_{\mathrm{L}})t_d-\phi_0\,\mathrm{sign}(\omega)$ [Eq. (3.2) of Ref. 13], one obtains Eq. (3.13) of Ref. 13. Equation (7) shows that for every value of t_d and an arbitrary spectral phase difference at zero delay, the phase-locked pulse pair signal depends only on those transitions in the absorption spectrum of the sample which can be excited by the single pulse spectrum. On physical grounds, we do not expect the experiment to measure the dispersive susceptibility because changes in μ_{ji} at frequen-

cies where $e(\omega_{ji})=0$ would alter the refractive index without affecting the signal.

The Kramers–Kronig relations connect the real and imaginary parts of the susceptibility over all frequencies. In principle, the imaginary susceptibility must be known at *all* frequencies to calculate the real susceptibility (e.g., ultraviolet absorption usually determines the visible refractive index of transparent materials). Aside from this breakdown of the Kramers–Kronig inversion for finite bandwidth data,[115] another reason for avoiding inadvertent Kramers–Kronig inversion of absorption/refractive index data is that the attenuation coefficient and refractive index each depend on both the real and imaginary parts of the susceptibility.[116,117] The imaginary part of the susceptibility is responsible for all transfer of energy between material and field, but the attenuation coefficient of metals includes reflection,[117] and metals obey a slightly different Kramers–Kronig relation.[116] From here on, the discussion is limited to dilute chromophores so that the imaginary susceptibility determines the absorption coefficient. In MKS units, the imaginary part of the susceptibility for the isolated molecules treated above is given by

$$\chi''(\omega)=2\pi\sum_{i,j} N_i\cdot|\mu_{ji}|^2[\delta(\omega-\omega_{ji})-\delta(\omega+\omega_{ji})]/\epsilon_0\hbar, \tag{8}$$

where ϵ_0 is the permittivity of vacuum. The imaginary part of the susceptibility is an odd function of frequency. Since the separation of absorption and dispersion is simplest in the complex frequency domain, a frequency domain picture is useful for understanding the absorption/dispersion content of time domain experiments. The absorption coefficient alters the field amplitude, so it must be an even function of frequency (and lead to even time domain signals for an ideal Mach–Zehnder interferometer in which $\Delta\phi(\omega)\equiv\omega t_{\text{delay}}$). The absorption coefficient is given by $N\sigma(\omega)=\omega\chi''(\omega)/n(\omega)c$ where N is the total molecular density, σ is the absorption cross-section, n is the refractive index, and c is the speed of light.[118] In contrast, the refractive index alters the spectral phase in the form $\phi(\omega)=(n(\omega)-1)l\omega/c$ as an odd function of frequency. The even/odd properties of the absorptive/dispersive observables are opposite those of the corresponding susceptibilities, which reflects the $\pi/2$ phase lag between the emitted electric field and the source polarization at each frequency.

The complex Fourier transform of the Nyquist sampled pulse pair excited state population interference signal given by Eq. (7) is:

$$\begin{aligned}
&\int_{-\infty}^{\infty} P^{\text{int}}(t)\exp(i\omega t)dt \\
&\quad=2\pi V\sum_{i,j} N_i\cdot|\mu_{ji}e(\omega_{ji})/\hbar|^2 \\
&\qquad\times\{\delta(\omega-\omega_{ji})\exp[-i\phi_0(\omega_{ji})] \\
&\qquad+\delta(\omega+\omega_{ji})\exp[i\phi_0(\omega_{ji})]\} \\
&\quad=\{(\epsilon_0 V\cdot[\omega\chi''(\omega)]\cdot|e(\omega)|^2)/(n(\omega)|\hbar\omega|)\} \\
&\qquad\times\exp[-i\phi_0(\omega)].
\end{aligned} \tag{9a}$$

The first equality in Eq. (9a) is the gas-phase isolated molecule result for an arbitrary spectral phase difference at $t=0$. The sum from Eq. (7) has been extended over all i using excited state populations $N_j=0$. To get the more general result for dilute chromophores in the second equality of Eq. (9a), the imaginary susceptibility in Eq. (8) was multiplied by the odd function $\omega/|\omega|$ in order to substitute $\omega\chi''(\omega)/|\omega|$ for the even function of frequency appearing on the first equality of Eq. (9a) and the refractive index was included. The absolute value of $\hbar\omega$ represents the photon energy. All of the results should be multiplied by $|\hbar\omega|$ if the absorbed energy were measured instead of excited state population. No matter what the spectral phase difference, *only* the absorption coefficient appears in the Fourier transform of the complete pulse pair signal. *By inversion of the Fourier transform, this implies that absorption determines the signal for every time delay, even with an arbitrary spectral phase difference.* The imaginary susceptibility and refractive index cannot be separated by sampling a reduced set of time delays or changing the spectral phase.

The population interference signals obtained for constant spectral phase shifts of 0 and $\pi/2$ by Fourier transformation of the second line of Eq. (9a) are given below. For $\phi_0(\omega)=0$, the signal is

$$\begin{aligned}
P_0^{\text{int}}(t)&=(1/2\pi)\int_{-\infty}^{\infty}\{(\epsilon_0 V\cdot[\omega\chi''(\omega)]\cdot|e(\omega)|^2)/ \\
&\qquad(n(\omega)|\hbar\omega|)\}\exp(-i\omega t)d\omega \\
&=1/\pi\int_0^{\infty}\{(\epsilon_0 V\cdot[\omega\chi''(\omega)]\cdot|e(\omega)|^2)/ \\
&\qquad(n(\omega)|\hbar\omega|)\}\cos(\omega t)d\omega,
\end{aligned} \tag{9b}$$

where the second equality is obtained from the first by noting that we are dealing with the Fourier transform of an even function of frequency. The $\phi_0(\omega)=0$ signal is an even function of pulse delay, as expected by symmetry. The case of a $\pi/2$ phase shift is slightly more complicated because then $\phi_0(\omega)=(\pi/2)\text{sign}(\omega)$. The sign function appears because the spectral phase is an odd function of frequency (as discussed in Sec. II). For a $\pi/2$ phase shift, we thus have $\exp[-i\phi_0(\omega)]=-i\,\text{sign}(\omega)$ so that we are taking the Fourier transform of an odd frequency domain function to obtain an odd time domain signal.

$$\begin{aligned}
P_{\pi/2}^{\text{int}}(t)&=(1/2\pi)\int_{-\infty}^{\infty}\{(\epsilon_0 V\cdot[\omega\chi''(\omega)] \\
&\qquad\cdot|e(\omega)|^2)/(n(\omega)|\hbar\omega|)\}[-i\,\text{sign}(\omega)] \\
&\qquad\times\exp(-i\omega t)d\omega \\
&=1/\pi\int_0^{\infty}\{(\epsilon_0 V\cdot[\varepsilon\chi''(\omega)]\cdot|e(\omega)|^2)/ \\
&\qquad(n(\omega)|\hbar\omega|)\}\sin(\omega t)d\omega.
\end{aligned} \tag{9c}$$

Although the second equality of Eq. (9c) looks like a truncated $(0,+\infty)$ Fourier sine transform of the absorption coef-

ficient, the first equality of Eq. (9c) shows that it actually represents the Fourier transform of an odd function over the entire $(-\infty, +\infty)$ real axis.

Experimentally, phase control can be used to manipulate how a frequency domain observable is transformed by a time domain measurement. Phase control *does not alter* the basic frequency domain quantity measured by an experiment. For example, $\phi_0=0$ phase-locked pulse pair absorption produces the Fourier cosine transform of the absorption coefficient while $\pi/2$ phase-locked pulse pair absorption appears to yield the Fourier sine transform of the absorption coefficient. The transforms used to analyze experimental data must match those performed by the experiment. The equations used in Ref. 13 to obtain the real or dispersive part of the susceptibility involve inverse cosine (sine) transformation of truncated odd (even) time domain signals over the range $(0, \infty)$. The full $(-\infty, +\infty)$ transforms are identically zero. It is shown in the appendix that these truncated Fourier transforms are mathematically equivalent to a Kramers–Kronig inversion of the absorption data. The dispersive susceptibility obtained from phase-locked pulse pair absorption is therefore calculated from finite bandwidth absorption data, *not* experimentally measured. Formally treating a pulse pair signal as causally restricted to positive times like a free induction decay can be very misleading if the signal exists for negative pulse delays.

Phase-locked pulse pairs can be useful for systematically undersampling Fourier transform spectra and for nonlinear spectroscopy when a timed measurement of the absorption spectrum is required. Corrections for interferometer imperfections and systematic undersampling are also likely to be useful. The absolute value of the Fourier transform of double sided interferograms [such as Eq. (9a)] had been used to correct interferometer imperfections in optical Fourier transform spectroscopy[37] but has been replaced by more sophisticated methods which determine the interferometer phase error from the interferogram itself and do not degrade the signal-to-noise.[38,119] The idea behind these methods is that the interferometer phase error is a slowly varying function of frequency which can be characterized by the coarsely sampled phase error $\delta\phi(\omega)=\arctan[\mathrm{Im}(S(\omega))/\mathrm{Re}(S(\omega))]$ obtained by Fourier transformation with respect to a small range of delays around zero.

By systematically sampling at intervals which are integer multiples of the locked frequency period, the method of phase-locked pulse pairs aliases both locked frequencies $(\pm\omega_L)$ to zero.[36] Equation (3.13) of Ref. 13 can be used for calculating the linear phase-locked pulse pair population interference signal with carrier wave delays and constant spectral phase-shifts. Sampling a carrier wave signal at times which differ by a quarter optical cycle can significantly alter the signal. Time domain pulse pair absorption signals calculated using carrier wave pulses with a constant $\pi/2$ spectral phase shift are contrasted with phase-locked pulse pair absorption signals for envelope delays $t_d=2\pi(m+1/4)/\omega_L$ in Fig. 5. For both signals, the frequency domain product which determines the signal is $\sigma(\nu)I(\nu)=\exp[-(\nu-\nu_1)^2/\Delta^2]$ where $\nu_1=136/512$ cycles/timestep and $\Delta=1/(10\pi\sqrt{3})$. The fractional bandwidth of $\Delta\omega/\omega_0\approx 0.11$ in Fig. 5 was selected

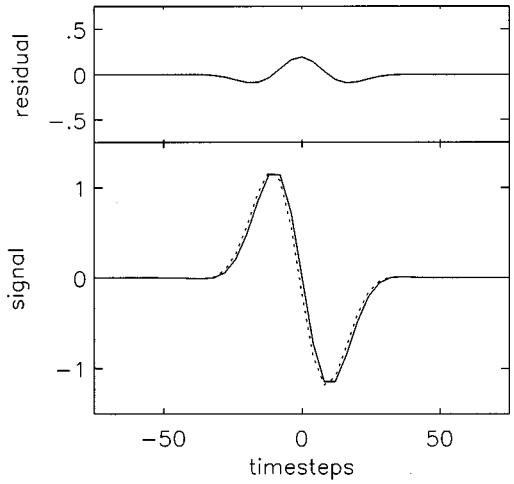

FIG. 5. Undersampled time domain pulse pair absorption signals generated using carrier wave delays with a $\pi/2$ spectral phase-shift (lower panel, solid curve) and phase-locked envelope delays which generate a $\pi/2$ carrier wave phase-shift by adding an extra quarter-cycle of delay (lower panel, dotted curve). Both transients sample the same carrier wave signal at different times. Undersampling is apparent in the line segments connecting data points. The difference between these two signals is plotted on the same vertical scale in the upper panel. Near time zero, the difference between carrier wave and phase-locked signals amounts to 20% of the maximum signal. If a unit time step in the figure corresponds to 0.7 fs, the time domain signals approximate those generated from the spectrum of a 10 fs Gaussian pulse centered at 800 nm with the carrier and locked frequencies both set at 850 nm (i.e., the product (absorption cross-section)×(pulse spectrum) which determines the signal has the shape of a 10 fs Gaussian pulse).

to match the fraction (full width at half maximum/carrier frequency) for a 10 fs Gaussian pulse centered at 800 nm. The carrier frequency ν_0 of the carrier wave pulses is set equal to the locked frequency ν_L of the phase-locked pulses. $\nu_0=\nu_L=1/4$ cycle/timestep. Both signals are plotted as a function of the integer number of timesteps, m. The solid curve is generated from carrier wave delays sampled at the carrier period with $\pi/2$ spectral phase shift using delays $t_d=4m$. The dotted curve is calculated at the envelope delays $t_d=(4m+1)$ used in a phase-locked pulse pair experiment. The extra quarter-cycle of envelope delay in a phase-locked experiment generates a $\pi/2$ carrier wave phase shift. If plotted as a function of delay, both signals would lie on the fully sampled carrier wave signal, but at different delays. The difference between signals is concentrated around time zero and amounts to 20% of the maximum signal in this case. The maximum possible difference depends on the fractional bandwidth roughly as $\sin[(\pi/2)(\Delta\omega/\omega_0)]$ and is expected to be less than 3% for the experiments on gas-phase I_2. Explicit inclusion of the extra quarter cycle delay in the $\pi/2$ transient can reduce or eliminate the effect of this difference on the recovered absorption cross section (see below).

Figure 6 illustrates the difference between the time domain pulse pair signals calculated for envelope delays with relative phase $\phi_0=0$ (panel A), carrier wave delays with relative phase $\phi_0=0$ (panel B), and carrier wave delays with relative phase $\pi/2$ (panel C). The sampling rate is the same in all three panels. All three signals are determined by the same (absorption spectrum)×(pulse spectrum) product given by $\sigma(\nu)I(\nu)=[\delta(\nu_1)+2\delta(\nu_2)]\otimes\exp(-\nu^2/\Delta^2)$ where ν_1

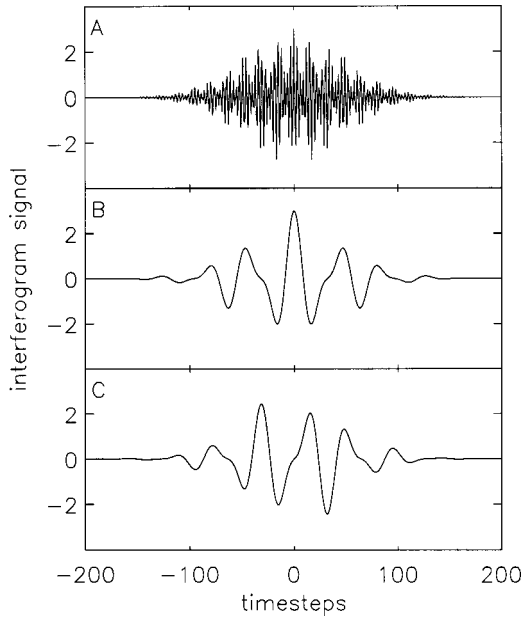

FIG. 6. Comparison of the time domain pulse pair absorption signals for envelope delays (panel A) and carrier wave delays with phase shifts of $\phi_0=0$ (panel B) and $\phi_0=\pi/2$ (panel C). The signals in all three panels measure the common (absorption spectrum)×(pulse spectrum) product given by $\sigma(\nu)I(\nu)=[\delta(\nu_1)+2\delta(\nu_2)]\otimes\exp(-\nu^2/\Delta^2)$ where $\nu_1=135/512$, $\nu_2=167/512$, and $\Delta=1/(\pi\tau)$ with $\tau=70$. The sampling rate is the same in all panels. The signal generated using envelope delays (panel A) exhibits interferometric oscillations at both ν_1 and ν_2 and is symmetric about $t=0$ because the pulses are identical. The carrier wave signals were generated with a carrier frequency $\nu_0=155/512$, which is aliased to zero. The signal generated with carrier wave pulse delays for relative phase $\phi_0=0$ (panel B) is also symmetric about $t=0$ but has no interferometric oscillations. Panel C shows the signal generated with carrier wave pulse delays and a relative phase $\phi_0=\pi/2$, which is antisymmetric about $t=0$ and has no interferometric oscillations. The equations used for generating each signal are given in the text.

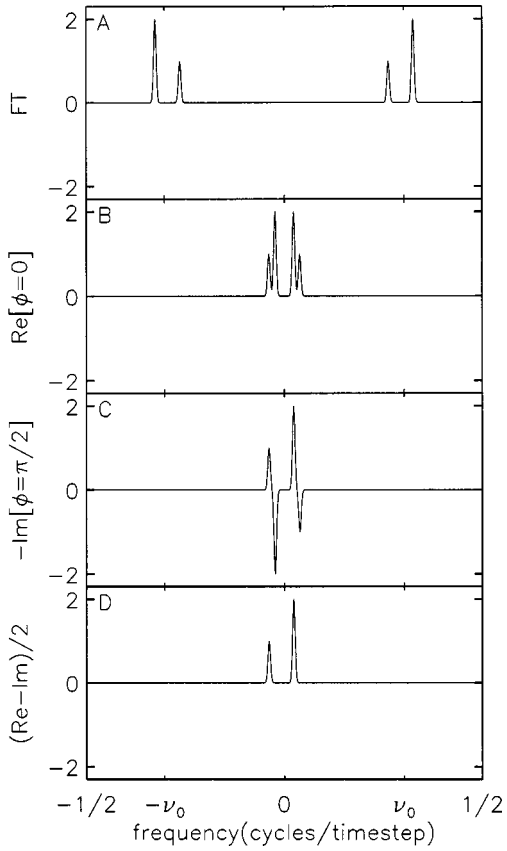

FIG. 7. Inverse Fourier transforms of the pulse pair signals shown in Fig. 6 demonstrate the aliasing of the carrier frequency to zero. All four panels are plotted vs. the frequency axis generated by Fourier transforming the time axis in Fig. 6. Panel A is the full inverse Fourier transform of panel A of Fig. 6 and shows that both frequencies ($\nu_1=135/512$ and $\nu_2=167/512$) are recovered on each side of zero. Panel B is the real part of the inverse Fourier transform of the carrier wave delay signal with $\phi=0$ from panel B in Fig. 6. The imaginary part of the transform is zero. Both the positive and negative frequency spectra in panel A have been shifted toward zero by the carrier frequency. The carrier frequency, $\nu_0=155/512$, is referenced for visual aid on each side of zero. The peak at $\nu_2=167/512$ in panel A is located at $\nu_2-\nu_0=12/512$ in panel B, the peak at $-\nu_2=-167/512$ in panel A is at $-(\nu_2-\nu_0)=-12/512$ in panel B, and the peaks at $\pm135/512$ in panel A are located on the other side of zero at $\pm(\nu_1-\nu_0)=\mp20/512$. From the spectrum in panel B, one cannot determine whether a given frequency lies above or below the carrier frequency. Panel C shows the negative of the imaginary part of the inverse Fourier transform of the data from panel C in Fig. 6. The real part of this transform is zero. Both the positive and negative frequency spectra in panel A have been shifted toward zero by the carrier frequency, but negative frequency components in panel A have a negative sign in panel C. Panel D shows the shifted spectrum recovered by combining the real and imaginary parts given in panels B and C, $(\mathrm{Re}[\phi=0]-\mathrm{Im}[\phi=\pi/2])/2$, and demonstrates the aliasing of the carrier frequency on the zero point, resulting in peaks at $\nu-\nu_0=-20/512$ and 12/512 instead of the actual frequency values of 135/512 and 167/512. Adding the spectra in panels B and C cancels the aliased negative frequency components in panel A and leaves only the aliased positive frequency components. The spectrum in panel D can be shifted up by the carrier frequency to obtain the positive frequency spectrum in panel A.

$=135/512$, $\nu_2=167/512$, and $\Delta=1/(\pi\tau)$ with $\tau=70$. The $\phi_0=0$ envelope pulse delay signal in panel A is given by $[\cos(2\pi\nu_1 t)+2\cos(2\pi\nu_2 t)]\exp[-t^2/\tau^2]$. The $\phi_0=0$ carrier wave signal in panel B is given by $[\cos(2\pi(\nu_1-\nu_0)t)+2\cos(2\pi(\nu_2-\nu_0)t)]\exp[-t^2/\tau^2]$ with carrier wave frequency $\nu_0=155/512$. The $\pi/2$ phase shifted carrier wave signal in panel C is given by $[\sin(2\pi(\nu_1-\nu_0)t)+2\sin(2\pi(\nu_2-\nu_0)t)]\exp[-t^2/\tau^2]$. Note the even time symmetry of the two $\phi_0=0$ transients (panels A and B) and the absence of high frequency oscillations in the two carrier wave transients (panels B and C). The sampling rate is the same in all three cases, but a lower sampling interval $[\sim 1/2(\nu_2-\nu_1)]$ would be sufficient to fully characterize the signals generated with carrier wave delays.

Figure 7 shows the inverse Fourier transforms of the data in Fig. 6 and illustrates the aliasing that occurs when carrier wave delays are used instead of envelope delays. The absolute value power spectrum of any real time domain signal is symmetrical about zero frequency. Systematic undersampling (above the critical undersampling frequency dictated by twice the excitation pulse bandwidth) also produces a symmetrical power spectrum with positive frequencies translated to $\omega-\omega_L$ and negative frequencies translated to $\omega+\omega_L$.[36] A single undersampled signal provides no information about whether a given frequency in the aliased power spectrum lies above or below the locked frequency in the absorption spectrum of the sample. One solution (which has some similarities to heterodyne detection in magnetic resonance)[24] would be to set the locked frequency to one (known) side of all excited sample frequencies. Another way to resolve this ambiguity is to record two interference

signals with relative spectral phases between the pulses in the pulse pair of 0 (panel B) and $\pi/2$ (panel C). This has similarities to quadrature detection in magnetic resonance.[24] Since the interference population is an even function of t_d for $\phi_0=0$ (with an even inverse Fourier transform as a function of frequency) and an odd function of t_d for a $\pi/2$ phase shift (with an odd inverse Fourier transform as a function of frequency), the difference of the two discrete inverse Fourier transforms has amplitude only from positive frequencies aliased to $\omega-\omega_L$ and can thus provide the absorptive susceptibility for positive frequencies within the bandwidth of the pulse

$$\chi''(\omega-\omega_L)|e(\omega-\omega_L)|^2 = \left(\sum_t P_0^{\mathrm{int}}(t)\cos(\omega t)-\sum_t P_{\pi/2}^{\mathrm{int}}(t)\sin(\omega t)\right)\hbar/(\epsilon_0 V). \tag{10}$$

The results of the subtraction in Eq. (10) are shown in panel D of Fig. 7. This use of unshifted and $\pi/2$ phase shifted pulse pairs to determine whether frequencies lie above or below the carrier frequency is reminiscent of phase cycling in NMR.[25] Equation (10), the final result of this analysis, agrees with Eq. (3.26) of Ref. 13. As shown in the appendix, the calculation used in Ref. 13 to obtain the dispersive part of the linear susceptibility is equivalent to Kramers–Kronig inversion of Eq. (10). In the dilute gas phase, the absorptive susceptibility is necessary and sufficient to predict the phase-locked transients.

It might be supposed that Kramers–Kronig inversion would allow a complete description of the phase-locked transients using the dispersive susceptibility. However, the dispersive susceptibility [or the resonant contribution obtained from Eq. (3.27) of Ref. 13] does not depend on and cannot predict the $\phi=0$ transient at delay $t=0$. This $t=0$ data point provides the frequency integral of the absorption spectrum, which is needed to recover any unresolved or constant background terms in the spectrum, and is not reflected in the dispersive susceptibility.[112] (The Hilbert transform of a constant is zero.) The dispersive susceptibility is not necessary and not sufficient to calculate phase-locked transients.

The above discussion was based on the use of pulses with a constant spectral phase-shift at the same delay when the method of phase-locked pulse pairs uses a quarter cycle delay to generate a $\pi/2$ carrier wave phase-shift. This extra delay was included in the Riemann sums used to evaluate Eq. (3.26) in Ref. 13 so that any residual error in $\chi''(\omega)$ results only from finite stepsize.[120] Remarkably, the fast Fourier transform methods used to correct interferometer imperfections in Fourier transform spectroscopy can be used to shift the sampling times. Figure 8 illustrates how the substitution of a quarter-cycle envelope delay for a $\pi/2$ spectral phase-shift affects the inverse Fourier transforms of the two time domain signals shown in Fig. 5. The relatively large differences in the time domain signal are transformed into a systematic error in partitioning the signal between the real and imaginary parts of the complex frequency domain transform. The absolute value of the frequency domain signal is unaffected. Because the difference in spectral phase between

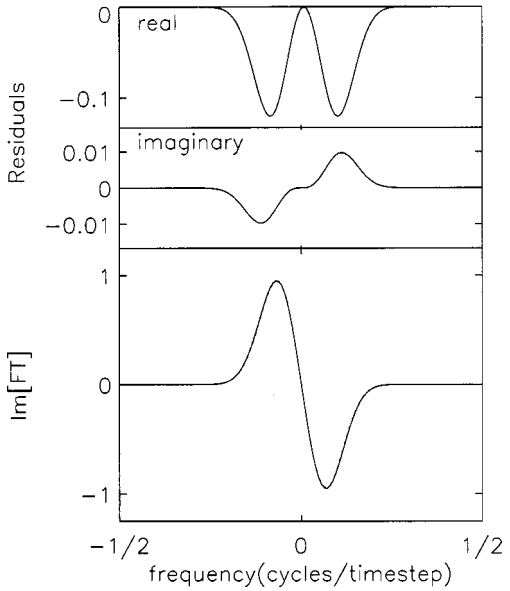

FIG. 8. The imaginary parts of the inverse fast Fourier transforms (FFT) of the $\pi/2$ phase shifted carrier wave and $\pi/2$ phase locked signals in Fig. 5 are overlaid in the lower panel (and are almost indistinguishable). The two traces have systematic differences plotted in the top panels. The residuals are plotted on different scales so that their shape can be seen. The error in the inverse FFT of the phase-locked signal lies mainly in the real part. The inverse FFT of the carrier wave delay signal has no real part whereas the inverse FFT of the signal generated with phase-locked pulses (using a quarter-cycle envelope delay to generate a $\pi/2$ carrier wave phase shift) has a real part which exceeds 10% of the maximum imaginary part. The error in the inverse FFT of the $\pi/2$ phase-locked envelope delay signal can be corrected as if it were an interferometer imperfection using equations given in the text, thus allowing correction of the time domain transient as well.

a quarter-cycle delay and a $\pi/2$ phase shift, $\delta\phi(\omega)=(\pi/2)\times(1-\omega/\omega_L)$, is independent of delay throughout the quadrature signal, it can be regarded as an extra interferometer phase error in the quadrature signal. Since the phase-locked pulse pair transient is undersampled so that ω_L is aliased to zero, the phase correction must also be shifted by ω_L. In terms of the aliased frequency axis, the phase error is given by $\delta\phi(\omega)=(\pi/2)(\omega/\omega_L)$. This provides a way to phase correct undersampled phase-locked $\pi/2$ transients for the extra quarter-cycle delay. We have verified that this procedure numerically corrects the inverse Fourier transform of the interferogram in Fig. 5 to within machine precision as expected from Nyquist's theorem.[36] If other sources of interferometer phase error are accurately known, the inverse Fourier transforms of undersampled $\phi_0=0$ and $\pi/2$ transients (recorded with phase-locked pulse pairs) can each be numerically phase corrected and subtracted to yield the absorption spectrum.

C. Nonlinear spectroscopy

When envelope pulse delays generated by an optical delay line (no envelope phase-shift as a function of delay) are used, the electric field of a delayed pulse is given by substituting $t-t_d$ everywhere in $E(t)$. If the nonlinear polarization can be expanded in a functional power series,[121] the third-order polarization can be written as a convolution of the third-order impulse response with three optical electric

fields.[28,122] For a causal third-order nonlinear response in a homogeneous and isotropic medium, the nonlinear polarization in four-wave mixing is given by:

$$P^{(3)}(\vec{r},t,t_a,t_b)=\int_0^\infty\int_0^\infty\int_0^\infty \chi^{(3)}(\tau_a,\tau_b,\tau_c) \times E_a(t-t_a-\vec{k}_a\cdot\vec{r}/\omega_a-\tau_a) \times E_b(t-t_b-\vec{k}_b\cdot\vec{r}/\omega_b-\tau_b) \times E_c(t-\vec{k}_c\cdot\vec{r}/\omega_c-\tau_c)d\tau_a d\tau_b d\tau_c. \quad (11)$$

The third-order response function $\chi^{(3)}(\tau_a,\tau_b,\tau_c)$ is equal to the polarization created by three delta function excitation pulses at the times τ_a, τ_b, and τ_c before the present. At $\vec{r}=0$, pulses *a* and *b* are centered at $t=t_a$ and $t=t_b$, and the zero of time *t* is referenced to the center of pulse *c* (i.e., $t_c=0$). Dispersion in the sample has been neglected. Equation (11) does not automatically incorporate macroscopic phase-matched signal generation. A procedure for spatial averaging is given by Abella *et al.*[49] Envelope pulse delays allow a complex triple inverse Fourier transformation with respect to t_a $(-\omega_a)$, t_b (ω_b), and t $(\omega_c+\omega_b-\omega_a)$. The Fourier transform frequency variable conjugate to each time variable is listed after it in parentheses. The frequency variables used in the transformations with respect to t_a, t_b, and t above were chosen so that the sign s_i of the frequency ω_i $(i=a, b,$ or $c)$ in the signal frequency $\omega_s=\Sigma s_i\omega_i$, matched the sign of the excitation pulse wave-vector $\vec{k}_i$ in the wave-vector of the signal, $\vec{k}_s=\Sigma s_i\vec{k}_i$. An interchange of the order of integration for each transform yields the complex polarization in the frequency domain

$$\hat{P}^{(3)}(\vec{r},(\omega_c+\omega_b-\omega_a),-\omega_a,\omega_b) =\hat{\chi}^{(3)}(-\omega_a,\omega_b,\omega_c)\hat{E}_a(-\omega_a)\hat{E}_b(\omega_b)\hat{E}_c(\omega_c) \times\exp[i(\vec{k}_c+\vec{k}_b-\vec{k}_a)\cdot\vec{r}], \quad (12)$$

where $\hat{\chi}^{(3)}$ is the complex half inverse Fourier transform (0, ∞) of the third-order response function $\chi^{(3)}$ with respect to τ_a, τ_b, and τ_c. The frequency variables used for t_a, t_b, and *t* dictated the conjugate Fourier transform frequencies for τ_a $(-\omega_a)$, τ_b (ω_b), and τ_c (ω_c). According to Eq. (12), constant spectral phase shifts ϕ_i of the excitation pulses produce a constant spectral phase shift $\phi_s=\Sigma s_i\phi_i$ of the source polarization. Constant spectral phase shifts thus allow a generalization of the phase cycling techniques used in magnetic resonance[10,24,25,123] to frequency modulated pulses.

Equation (12) is an equivalent description of the polarization in terms of the frequency domain third-order nonlinear susceptibility $\hat{\chi}^{(3)}$, which is a function of three independent frequencies, each of which has domain $(-\infty, +\infty)$.[116,122] This suggests that efficient triple Fourier transform algorithms can replace the time consuming triple convolutions currently used to calculate femtosecond four-wave mixing signals. The corresponding triple Fourier transform is not straightforward for carrier wave delays (no carrier wave phase-shift as a function of delay), essentially because the pulse spectra depend on the delays. The third-order susceptibility also provides a way to discuss the absorption/dispersion information content of four-wave mixing experiments in the frequency domain.

Because time domain polarizations and optical fields are real, the third-order impulse response is also real.[28,116,122] This fact is sometimes obscured by use of complex fields and the rotating wave approximation to simplify calculations, but was explicitly discussed in the article by Cho *et al.* proposing the ''three pulse phase-locked pump–probe absorption'' and ''phase-locked heterodyne detected stimulated photon echo'' experiments.[14] Real parts of the nonlinear susceptibility describe interactions which involve no net change of the material energy, but may exchange energy between electromagnetic waves (e.g., second harmonic generation in transparent nonlinear crystals). Imaginary parts of the nonlinear susceptibility involve exchange of energy between the material and the electromagnetic waves (e.g., nonlinear absorption). Note that Raman transitions produced by off-resonant pulses involve imaginary parts of the nonlinear susceptibility.[124] Energy conservation in off-resonant four-wave mixing has been carefully discussed by Lee and Albrecht.[125] Since there is only one requirement that the triple Fourier transform of the third-order susceptibility be real, the real and imaginary parts of the third-order susceptibility obey less restrictive symmetry relations than the linear susceptibility $\hat{\chi}^{(3)}(\omega_1,\omega_2,\omega_3)^*=\hat{\chi}^{(3)}(-\omega_1,-\omega_2,-\omega_3)$.[116,122] Changing the sign of a single frequency does not necessarily produce a symmetry related susceptibility: the signs of all three frequencies must change.

The above development is of general applicability but is very formal. The monograph by Mukamel[28] describes how, within the rotating wave approximation, the time domain impulse response can be represented by a set of double sided Feynman diagrams which automatically incorporate macroscopic phase matching. As a representation of a single term in time dependent density matrix perturbation theory, each diagram has a specific order of interaction with the excitation pulses (which may not coincide with the pulse order if the pulses overlap in time). Mukamel and co-workers have developed useful approximate response functions for the contribution of each diagram to the third-order response which are widely used in femtosecond nonlinear optics.[27,28,61–65,126] The fields and response functions used in this formalism are complex-valued due to the rotating wave approximation. The equations for calculating the nonlinear polarization from the response functions in Mukamel's monograph[28] and articles[61–65] uniformly assume carrier wave delays, as do the equations used to invert frequency resolved optical gating (FROG) transients.[127–135] The modifications required for envelope delays will be briefly presented here. Equation (10.13) of Mukamel's monograph[28] gives the third-order polarization with wavevector $\vec{k}_s=\vec{k}_c+\vec{k}_b-\vec{k}_a$ generated by three noncollinear, noncoincident pulses with carrier wave delays t_a, t_b, and $t_c=0$ which interact with the sample in the order *a,b,c* as

$$\hat{P}^{(3)}(\vec{k}_s,t,t_a,t_b)$$
$$=(i/\hbar)^3\int_0^\infty dt_3\int_0^\infty dt_2\int_0^\infty dt_1[R_2(t_3,t_2,t_1)$$
$$+R_3(t_3,t_2,t_1)]\hat{e}_c(t-t_3)\hat{e}_b(t-t_b-t_3-t_2)$$
$$\times\hat{e}_a^*(t-t_a-t_3-t_2-t_1)\exp[i\omega_c t_3]$$
$$\times\exp[i\omega_b(t_3+t_2)]\exp[-i\omega_a(t_3+t_2+t_1)]. \quad (13)$$

Equation (13) is the only numbered equation given in this article for carrier wave delays. In Eq. (13), t_1, t_2, and t_3 label positive time intervals between the four perturbation theoretic field–matter interactions (one with each pulse plus signal emission). $\hat{e}(t)$ designates a complex pulse envelope centered at $t=0$ (so that pulses *a*, *b*, and *c* are centered at times t_a, t_b, and 0, respectively). In terms of the real temporal envelope $e(t)$ and temporal phase $\phi(t)$ defined in Eq. (1), the complex envelope of a carrier wave delayed pulse is given by $\hat{e}(t)=(1/2)e(t)\exp[i(\phi(t)-\omega_0 t)]$ so that $E(t-t_d)=[\hat{e}(t-t_d)\exp(i\omega_0 t)+\text{c.c.}]$ where ω_0 is the carrier frequency. The complex third-order impulse response functions R_2 and R_3 are given by the superoperators $\text{Tr}[G_{\text{eg}}(t_3)\times G_{\text{ee}}(t_2)G_{\text{ge}}(t_1)\rho_{\text{EQ}}]$ and $\text{Tr}[G_{\text{eg}}(t_3)G_{\text{gg}}(t_2)G_{\text{ge}}(t_1)\rho_{\text{EQ}}]$ [Mukamel Eq. (7.11)][28] where G_{xy} is a Green function for the set of density matrix elements indicated by the subscripts (''*e*'' for excited electronic state, ''*g*'' for ground). The Green function $G_{xy}(t)$ is defined by Eq. (7.5) of Mukamel's monograph[28] and contains a factor $\exp(-i\omega_{xy}t)$ oscillating at the Bohr frequency $\omega_{xy}=(E_x-E_y)/\hbar$.

We find it convenient to retain labels *a*, *b*, and *c* for the three pulses (which are distinguished by their wave vectors). The indices 1, 2, and 3 refer only to the three ordered positive time intervals between perturbation theoretic field–matter interactions. When the excitation pulses overlap in time, the field interaction order need not coincide with the pulse order and additional response functions which represent other double sided Feynman diagrams contribute to the nonlinear polarization.[136,137] The *a,b,c* labels are convenient for such calculations. Equation (13) is identical to Eq. (10.13) of Mukamel's monograph if we set $t_a=-(\tau+\tau')$, $t_b=-\tau$, and subsequently replace the *a,b,c* pulse labels with 1, 2, 3. Equation (13) can be understood as calculating the complex time domain envelope of the third-order polarization $\hat{P}^{(3)}$ with carrier frequency $(\omega_c+\omega_b-\omega_a)$ for excitation pulses which have no carrier wave phase-shift as a function of delay. The real polarization is given by $P^{(3)}=\{\hat{P}^{(3)}(t)\exp[-i(\omega_c+\omega_b-\omega_c)t]+\text{complex conjugate}\}$. The envelope $\hat{P}^{(3)}$ is complex-valued when the instantaneous frequency of the real third-order polarization $P^{(3)}$ differs from the carrier frequency $(\omega_c+\omega_b-\omega_a)$. In contrast to the real and imaginary parts of the susceptibility, the real and imaginary parts of the complex time domain response functions and polarization envelope are *not* simply related to the dispersive and absorptive response.

It is important to note that the polarization calculated from Eq. (13) depends on the pulse delays t_a and t_b only through the position of the pulse envelopes and not through the oscillating terms. The delays t_a and t_b control the range of values of t_1 and t_2 that contribute to the polarization, but the field oscillations at the carrier frequency are exactly canceled by the electronic oscillations of the Green functions when the carrier frequency is tuned to resonance. At resonance, Eq. (13) predicts that the Fourier transform of the third-order polarization with respect to $\tau\equiv t_b-t_a$ should be centered near $\omega_\tau=0$. This prediction is correct for carrier wave delays, but not envelope delays (see below).

For pulses generated by an optical delay line (constant envelope phase), Eq. (13) for the third-order polarization with wave vector $\vec{k}_s=\vec{k}_c+\vec{k}_b-\vec{k}_a$ generated by three noncollinear, noncoincident pulses which interact with the sample in the order *a,b,c* should be replaced by

$$P^{(3)}(\vec{k}_s,t,t_a,t_b,t_c)$$
$$=(i/\hbar)^3\int_0^\infty dt_3\int_0^\infty dt_2\int_0^\infty dt_1[R_2(t_3,t_2,t_1)$$
$$+R_3(t_3,t_2,t_1)]\hat{e}_c(t-t_c-t_3)\hat{e}_b(t-t_b-t_3-t_2)$$
$$\times\hat{e}_a^*(t-t_a-t_3-t_2-t_1)\exp[-i\omega_c(t-t_c-t_3)]$$
$$\times\exp[-i\omega_b(t-t_b-t_3-t_2)]$$
$$\times\exp[i\omega_a(t-t_a-t_3-t_2-t_1)]$$
$$+(\text{complex conjugate}). \quad (14)$$

Except for the nonlinear polarization, all of the variables in Eq. (14) have the same meaning as in Eq. (13). The time t_c represents the center of pulse *c*. The polarization P_3 calculated by Eq. (14) is real and oscillates at the actual instantaneous emission frequency. The addition of the complex conjugate in Eq. (14) is not related to the absorptive or dispersive response, but is simply the result of rotating wave approximations which yield complex time domain fields, $[\hat{e}(t)\exp(i\omega_0 t)]$, and response functions R_2 and R_3. The complete time domain field $E(t)$ and response function $\chi^{(3)}$ are both real. The response functions R_2 and R_3 oscillate at electronic frequencies during the t_1 and t_3 intervals so as to approximately cancel resonant field oscillations. *In contrast to Eq. (13), the polarization calculated by Eq. (14) contains oscillatory terms which depend on the pulse delays t_a and t_b.* In the fully noncollinear case, these optical frequency oscillations occur only in the phase of the polarization and not in the amplitude. The π spectral phase shift demonstrated in Fig. 3 is a consequence of Eq. (14). An analogous delay dependent phase modulation occurs in noncollinear second harmonic generation,[138] and was used by Joffre and coworkers to map the absolute value of the 2D second-order nonlinear response of a potassium di-hydrogen phosphate (KDP) doubling crystal.[68] Assuming perfect phase matching, the emitted third-order signal field $E^{(3)}$ has a $\pi/2$ phase lag behind the source polarization $P^{(3)}$ at each frequency. If the phase of the emitted signal field is measured, Eq. (14) predicts that the inverse Fourier transform of the third-order signal field $E^{(3)}$ with respect to $\tau\equiv t_a-t_b$ should be centered near $\omega_\tau=\pm\omega_{eg}$ where ω_{eg} is the electronic Bohr frequency. This has been experimentally observed by Hybl *et al.* in two-dimensional electronic spectra.[43]

The relationship between the individual complex conjugate components of the third-order polarization given by Eq. (13) and Eq. (14) is a multiplication by functions which can be pulled outside the integral [e.g., $\exp[i(\omega_c t_c+\omega_b t_b-\omega_a t_a)]$ for the term written out in Eq. (14)]. Using the inverse Fourier shift theorem, this multiplication will shift the Fourier transform of the signal field by the carrier frequency. Just as illustrated in Fig. 7 for linear phase-locked pulse pair absorption, carrier wave delays will produce a 2D spectrum in which both positive and negative carrier frequencies are shifted to $\omega_\tau=0$. Depending on how the signals are experimentally generated and detected, these shifts can overlap different quadrants of a 2D spectrum. As in the linear phase-locked pulse pair experiment, this overlapping of different quadrants can be removed by a phase cycling procedure (see below).

The differences between Eq. (13) (carrier wave delays) and Eq. (14) (envelope delays) become important whenever the phase of the nonlinear signal is measured,[42,43] or the signal contains interferometric oscillations. Equation (14) has the property that for envelope delay delta function pulse envelopes $[E(t)=e_0\delta(t)]$, the nonlinear polarization is given directly by the impulse response functions, i.e.,

$$P^{(3)}(\vec{k}_s,t,t_a,t_b,t_c)=\{(i/\hbar)^3[R_2(t-t_c,t_c-t_b,t_b-t_a)+R_3(t-t_c,t_c-t_b,t_b-t_a)]e_c e_b e_a^*+\text{c.c.}\}. \quad (15)$$

There is no phase factor which depends on the pulse delay. Equation (14) must be used to calculate the experimental 2D Fourier transform spectra obtained with optical delay lines.[43] Gallagher Faeder and Jonas[66,67] have used Eq. (14) (and analogous equations for the other Feynman diagrams) to successfully calculate real and imaginary parts of the two-dimensional Fourier transform electronic spectra of IR 144 in methanol.

In the impulsive limit, Eq. (15) shows that the 2D spectra for envelope delays may be calculated by Fourier transformation of the third-order response functions, as was done by Hybl *et al.*[43] A recent article by Zhang, Chernyak, and Mukamel[45] gives expressions for quasi-impulsive 2D optical signals using carrier wave delays and emphasizes that a systematic, delay dependent choice of the relative pulse phases is needed to recover signals which are directly related to the response functions. Viewed as carrier wave delayed pulses, envelope delayed pulses have a systematic, delay dependent phase shift $\phi=\omega_0 t_d$ determined by the carrier frequency. A zero carrier frequency (effectively putting all of the field oscillations into the complex envelope) eliminates these delay dependent phase shifts. We note that all four delay dependent phase conditions [Eq. (C10) of Zhang, Chernyak, and Mukamel][45] are automatically met if the carrier frequency and all relative phase shifts are set to zero. Envelope pulse delays generated by an optical delay line automatically satisfy the special delay dependent phase conditions given by Zhang, Chernyak, and Mukamel[45] for carrier wave delayed pulses. Phase shifted pulses are not needed.

Many experiments in nonlinear optics[16,18,79–81] and coherent control[82–85] use phase-locked pulse pairs. The phase-locked heterodyne detected stimulated photon echo (HSPE) was proposed[14] and performed[16,18] as a method for separately measuring the real and imaginary parts of the third-order nonlinear response function. The separation discussed in these articles assumes carrier wave delays, a particular set of Liouville paths, the rotating wave approximation, and systematically undersampled data. The hypercomplex method given for separating the real and imaginary parts of 2D NMR spectra in the monograph by Ernst[25] is predicated on the same assumptions. The HSPE experiment requires two phase-locked pulse pairs (a total of four pulses). In the experiment, the sample is excited by one pulse pair (pulses *a* and *b*) and the change in transmitted power of the second pulse pair (pulses *c* and *d*) is measured as a function of the interpulse delays. The change in transmitted pulse pair power which depends on all four pulses is the HSPE signal.[18] de Boeij *et al.* demonstrated experimentally that HSPE signals depend on two separate phase shifts (ϕ_{ab} between the members of the first pulse pair and ϕ_{cd} between the members of the second pulse pair) and not just on their difference.[16,18] The separation of real and imaginary parts has been interpreted as a separation of the absorptive and dispersive parts of the material response,[14,28] and it has been stated that the HSPE provides the complete nonlinear response function of the system.[14,16,18,28] From a physical point of view, it is not clear how measurements of absorption of the second pulse pair can reflect changes in the refractive index of the sample caused by the first pulse pair.

It seems reasonable to investigate the sensitivity to dispersion during the first (indirectly detected) time interval by comparing to 2D NMR. Surprisingly, the question of whether the indirectly detected dimension of a 2D NMR spectrum actually measures the dispersive susceptibility seems to be open. A distinction between absorption and dispersion in each frequency dimension of four-wave mixing signals is not always physically significant. For example, resonance Raman scattering and resonance fluorescence are four-wave mixing processes[28] which can sometimes be phenomenologically distinguished by their detuning dependence. The Raman detuning dependence is dispersive (i.e., the frequency of the scattered light changes with excitation frequency) while the fluorescence detuning dependence is absorptive (i.e., the fluorescence frequency is determined by energy level differences which are independent of excitation frequency). Theoretical attempts to separate Raman and fluorescence have shown that the two processes interfere.[28,139,140] A distinction between Raman and fluorescence is physically sensible only when the interference can be neglected. This interference between Raman and fluorescence is an example which shows that one cannot always separate absorptive and dispersive intermediate steps in four-wave mixing. In general, only the total four-wave mixing process can be unambiguously characterized as dissipating field energy into the medium (imaginary part of frequency domain $\hat{\chi}^{(3)}$) or not (real $\hat{\chi}^{(3)}$). This distinction between absorption and dispersion becomes meaningful for each frequency dimension when nonlinear signals can be regarded as generated by sequential linear processes.

In nonlinear spectroscopy, the procedure for scanning

the time delays should be designed to avoid enforcing an artificial causality condition (and thus inadvertently introducing a Kramers–Kronig inversion of the data). The correct procedures are not always obvious. If a scan can somehow be extended to yield even time domain data, then a real frequency domain property of the sample (e.g., absorption coefficient) completely determines all the data on the entire time domain. Extensions of both pulse-pair time delays will be used in discussing the heterodyne detected stimulated photon echo. In some circumstances, the scan procedure discussed here for the HSPE experiment differs from that employed by the Wiersma group.[18]

The delays of an HSPE experiment can be scanned so that the delay $T \equiv \min(t_c,t_d) - \max(t_a,t_b)$ between the second pulse (a or b) in the first pulse pair (ab) and the first pulse (c or d) in the second pulse pair (cd) remains constant (and greater than or equal to zero). Experimentally, t_{ab} can be scanned over $(-\infty, +\infty)$ at constant T and constant t_{cd} by holding t_b, t_c, and t_d constant while scanning t_a from $-\infty$ to t_b, then holding t_a, t_c, and t_d constant while scanning t_b from t_a to $-\infty$. If the pulses in each pulse pair are identical ($\phi_{ab} = \phi_{cd} = 0$), then the HSPE signal is an even function of both delays between pulses in a pulse pair (t_{ab} and t_{cd}). This implies that the Fourier transform with respect to each pulse pair delay is an even and real function of frequency. A real 2D spectrum means that only the imaginary (energy dissipating) part of the frequency domain third-order susceptibility $\hat{\chi}^{(3)}$ is being probed for $\phi_{ab} = \phi_{cd} = 0$. Real 2D spectra are also interpreted as purely absorptive in 2D NMR.[24,25] When the first and second pulse pairs are so far apart that the susceptibility changes induced by the first pulse pair are stationary during the second pulse pair, the analysis of the linear phase-locked pulse pair experiments proves the HSPE signal is insensitive to refractive index changes (for all phase shifts ϕ_{cd}).[141] The last argument clearly establishes that the HSPE is blind to some refractive index changes which can be measured through scattering off a transient refractive index grating.[43,92,142,143] We therefore conclude the HSPE does not fully characterize the third-order nonlinear response observed in these fully noncollinear experiments.

At least in some circumstances, the absorptive polarization is selectively measured by HSPE experiments. A different interpretation of the real/imaginary separation proposed by Cho *et al.*[14] can be based on the complex envelope of the nonlinear polarization. Since phase-locking involves systematic undersampling of the electronic oscillations in the third-order response, two phase-cycled measurements are needed to determine whether *each* electronic frequency which would be observed in a fully sampled experiment lies above or below the locked frequency. The discussion of hypercomplex 2D NMR spectra in the monograph by Ernst[25] can be interpreted as a determination of whether indirectly detected frequencies lie above or below the carrier. In Eq. (13), these frequencies are embedded in the complex envelope of the third order polarization, so the determination of these frequencies and amplitudes appears to be a determination of the full complex envelope. This is not the case: for Eq. (13), a complex envelope is required to describe the absorptive nonlinear polarization in the presence of a Stokes' shift. The HSPE experiments[16,18] used phase-locking to approximate $\pi/2$ phase-shifts with quarter-cycle time delays. As in the linear experiments, this intrinsic phase-locking error can be estimated from the signal at a quarter cycle delay. For the model used by de Boeij *et al.* to simulate three pulse phase locked pump–probe experiments on DTTCI in ethylene glycol,[17] the signal at a quarter-cycle delay is calculated to be ~3% of the maximum signal for 20 fs pulses centered at 778 nm and a 760 nm locked frequency. There should be no interference signal at zero delay for a $\pi/2$ spectral phase-shift, so the intrinsic phase-locking error is about 3%. In the absence of interferometer imperfections (which may explain some departures from symmetry about $t = 0$ for the 0 phase data), the HSPE data all corresponds to the case $\phi_{ab} = \phi_{cd} = 0$. These HSPE experiments detect only the dissipative response, but this does not affect the primary quantity derived from the HSPE measurements, which is the instantaneous frequency of the nonlinear polarization.[18]

In contrast to HSPE experiments, refractive index changes contribute to fully noncollinear three pulse scattering signals.[43,142,143] Simulations of noncollinear experiments have used line shape functions which disagree with the linear absorption spectrum outside the spectral bandwidth of the excitation pulses.[136,137] Absorption coefficient and refractive index gratings contribute equally to the noncollinear transient grating signal pulse energy for an isolated transition probed by a resonant pulse which covers the entire transition.[43] This suggests that the sensitivity of noncollinear three pulse scattering experiments to refractive index changes caused by spectral changes outside the pulse spectrum is not properly accounted for in such simulations. Since the excited state absorption spectrum is often not known, the calculation of these refractive index changes may be problematic in some cases.

D. Homotime and heterotime detection

In time resolved optical spectroscopy, the phrase ''heterodyne detection'' has been used to describe any technique which amplifies a weak signal through interference with a reference.[28,144] In frequency domain spectroscopy, homodyne techniques (same frequency local oscillator) detect only one quadrature at a time and are distinguished from heterodyne techniques (different frequency local oscillator) which simultaneously detect both.[86] We have previously suggested that a time domain distinction between homodyne techniques (in which the local oscillator temporally overlaps the signal field) and heterodyne techniques (in which the local oscillator is temporally separated from the signal field) may be useful for time resolved spectroscopy. Since a different usage of heterodyne detection and homodyne detection is so entrenched in time resolved optical spectroscopy, it is probably not possible to restore the specific meanings they have in the frequency domain. However, the distinction has meaning for the measured physical properties, and it seems desirable to have names which both indicate what a technique measures and make a useful analogy to the frequency domain.

We suggest the terms homotime and heterotime detection to describe the corresponding time domain techniques

obtained from frequency domain homodyne and heterodyne techniques by swapping the words time and frequency everywhere in the frequency domain definition. When pulses overlap in time, the spectral phase difference due to delay is approximately constant over their bandwidth, and only one quadrature of the signal interferes with the reference (homotime detection). If the last excitation pulse is used as the local oscillator, only the absorptive quadrature is detected.[144] We propose to call use of the last excitation pulse as the local oscillator ''intrinsic homotime detection.'' With this classification, pump–probe[28] and three pulse phase-locked pump–probe[14,17,28] are examples of intrinsic homotime techniques. Note that the ''last excitation pulse'' and the ''local oscillator'' may be a pulse pair, as in the HSPE,[14,16,18,28] and it may be appropriate to rename HSPE as the ''homotime detected stimulated photon echo'' since it is an intrinsic homotime technique which probes the absorptive response to the second pulse pair. Fully noncollinear three pulse scattering techniques (e.g., transient grating scattering and stimulated photon echo) are sensitive to both absorption and refractive index gratings,[142,143] but do not separate the two quadratures. If the signal pulse is combined with a temporally overlapping local oscillator pulse outside the sample, then it is possible to measure both the absorptive and dispersive quadratures by shifting the phase of the local oscillator.[92] We suggest that use of an external, temporally overlapping local oscillator (which has strong similarities to quadrature detection in magnetic resonance) be called external homotime detection. Polarization spectroscopy[144,145] can be viewed as external homotime detection, since the signal and local oscillator (which is derived from the probe) have different polarizations before they are combined in the analyzing polarizer. When the signal is externally combined with a local oscillator pulse which is delayed by many pulse durations, the spectral phase from the delay varies rapidly with frequency and it is possible to separately recover both quadratures simultaneously by spectrally resolving the signal.[42,58] It seems natural to call this method external heterotime detection. The time based homotime/heterotime distinction proposed here has the advantage that heterotime techniques detect both absorption and refractive index changes simultaneously, homotime techniques detect only one quadrature at a time (absorption, dispersion, or some mixture), and intrinsic homotime techniques selectively recover only the absorptive quadrature.

E. Coherent control

Active ''coherent control'' of a chemical reaction always requires an interference between two pathways from reactants to products.[146] Two broad types of active optical control have been described in the literature.[6] The first set of schemes involves timed excitation of wavepackets and exploits interference between pathways that pass through different vibrational levels in the intermediate electronic states.[1,2] The addition of a constant spectral phase to any pulse has no effect on these experiments since a constant spectral phase does not affect the vibrational wavepacket evolution (which depends only on the relative spectral phases within the pulse bandwidth). The second class of coherent control experiments, which exploits interference between competing electronic pathways, is sensitive to the phase of a pulse which appears in only one of the two interfering paths.[3] For the latter class of coherent control experiments, the equations used to describe the delayed pulses must correspond to the experimental method of generating delays and phase-shifts in order to predict the observed experimental delay dependence ($\phi_0=0$ phase-locked experiments will be correctly predicted by either method). In particular, experiments with collinear pulses and envelope delays will yield interferometric oscillations which are out of phase in competing product channels. These interferometric oscillations are absent for carrier wave delays. The theoretical treatments in Refs. 70, 147 used envelope delays while Refs. 29–33 used carrier wave delays. Delays in the experiments described in Refs. 6, 110, 148–150 correspond to envelope delays. It is important to emphasize that even if an experiment generates pulses with carrier wave delays, pulses propagate in the sample with constant envelope phase (as long as dispersion can be neglected). If the pulses are collinear, every molecule in the sample sees the same interpulse delays and the same phase relationships between pulses. This simple physical picture shows clearly how theoretical proposals for two-photon interference control (e.g., $2\omega_0=\omega_+ +\omega_-$)[151] would work with macroscopic samples. While these two-photon schemes provide more complete control than the $\omega_3=3\omega_1$ schemes demonstrated so far,[6,152] they may be more vulnerable to dephasing in condensed matter.[153] Using carrier wave delays, Brown and Meath have theoretically investigated the phase-dependent effect of permanent dipole moments on the strong-field transition probability.[33] It is possible the phase dependence they report may be caused by microwave frequencies generated by the time domain phase-shift. For pulses which turn on or off in a few cycles, sensitivity to constant spectral phase-shifts (which do not change the frequency spectrum of a pulse) may be a useful criterion for electronic interference control and nonperturbative (strong field) effects.

VI. CONCLUSIONS

It is possible to define phase shifts and time delays either in terms of a carrier wave (which is natural in NMR) or in terms of the envelope of a single pulse (which is natural in optics). We have demonstrated that spectral interferometry can experimentally distinguish between a phase-shift and a time delay for 25 femtosecond pulses. Time delays were measured with a 1σ precision of 20 attoseconds ($\lambda/130$) and constant spectral phase-shifts are measured with a 1σ accuracy of 0.05 rad ($2\pi/120$). The 2σ accuracy of these measured constant spectral phase-shifts surpasses those reported by Xu *et al.*[34] with 8 fs pulses ($\pi/20$) and should improve as the pulse duration decreases. Constant spectral phase shifts were demonstrated by diffracting pulses from a variable phase volume diffraction grating.

The method of phase-locking femtosecond pulses introduced by Scherer *et al.*[11–13] involves addition of a small envelope delay generated by an interferometer to yield phase-shifts in the carrier wave sense. Phase-shifted carrier wave pulses allow systematic undersampling of rapidly oscillating

time-domain transients, but it is desirable to use phase-shifted pulses at the same delay (which requires constant spectral phase-shifts). A Fourier method was given for shifting phase-locked pulse pair signals to correct for the extra quarter-cycle envelope delay needed to produce a $\pi/2$ carrier wave phase-shift. Linear experiments with phase-locked pulse pairs are exactly equivalent to undersampled Fourier transform absorption spectroscopy and measure the absorption cross-section. Even with arbitrary control over the spectral phase, linear phase-locked pulse pairs cannot measure the refractive index or real part of the frequency domain susceptibility, but can deceptively Kramers–Kronig invert the product (absorption cross-section)×(pulse spectrum). The distinction between measured refractive indices and finite bandwidth Kramers–Kronig inversion is very important for experiments which exploit measurement of refractive indices to determine expansion of proteins[92] or are otherwise sensitive to changes in the absorption coefficient outside the pulse spectrum (e.g., noncollinear three-pulse scattering).[43,143]

The envelope time delays generated by an optical delay line were incorporated into the equations used to calculate femtosecond nonlinear optical signals (the usual equations assume carrier wave delays and yield correct results for experiments which are insensitive to the phase of the signal field). Envelope delays allow a straightforward triple Fourier transform of the time domain nonlinear response to yield a description of time domain experiments based on a three dimensional frequency domain susceptibility. For a fully noncollinear three-pulse scattering experiment, a constant spectral phase shift ϕ of any excitation pulse produces a constant spectral phase-shift $s\phi$ of the emitted nonlinear signal, where $s=\pm 1$ is the sign of the excitation pulse wave-vector in the signal wave-vector. A constant spectral phase shift thus generalizes the concept of time domain phase-shifts used in NMR phase cycling to arbitrary optical pulses. Equations for calculating time domain nonlinear optical signals with envelope pulse delays within the response function formalism of Mukamel were presented. The use of envelope pulse delays is crucial to calculation of interferometrically detected frequencies, since carrier wave delays alias the carrier frequency to zero and require phase cycling to determine whether an indirectly detected frequency lies above or below the carrier. In contrast, envelope pulse delays can recover indirectly detected frequencies without phase cycling. These envelope pulse delay equations are also needed to calculate the real and imaginary parts of two-dimensional Fourier transform spectra.[43,66,67] Experimental requirements for phase-resolved spectroscopy were outlined. The nonlinear optical properties measured with the phase-locked heterodyne detected stimulated photon echo were reexamined. In some circumstances (and possibly in general), the HSPE measures only the dissipative (imaginary) part of the third-order susceptibility. A more complete investigation of this point is needed. As in nonlinear optics, modifications of some equations used in the theory of coherent control are needed to match theory with experimental practice.

ACKNOWLEDGMENTS

We thank Arthur Pardi, Warren Warren, and Kurt Zilm for helpful discussions of magnetic resonance. We thank Paul Brumer and Robert Gordon for helpful discussions of coherent control. Ian Walmsley pointed out the zero frequency components generated by a pure time domain phase-shift during a stimulating conversation. We thank Graham Fleming for comments on a preliminary manuscript and Casey Hynes for comments on an early version of the appendix. We are grateful to Jeff Cina for more detailed comments and discussions. Allison Albrecht is an NSF Optical Science and Engineering Program graduate fellow. This work was supported by the Camille and Henry Dreyfus Foundation, the David and Lucile Packard Foundation, and the National Science Foundation.

APPENDIX

It is known that subjecting any even frequency domain function $f(\omega)$ to a Fourier cosine transform followed by an inverse Fourier sine transform is mathematically equivalent to Hilbert transformation (Kramers–Kronig inversion) of that function.[154] In magnetic resonance, Bartholdi and Ernst[112] have shown that supplementing a discretely sampled free induction decay with an equal number of zeroes before $t=0$ places the Hilbert transform of the absorption (dispersion) mode spectrum into every other data point of the dispersion (absorption) mode spectrum. The demonstration given here pays careful attention to the principal value character of the Kramers–Kronig inversion and emphasizes the contradiction inherent in ignoring the even or odd symmetry of a time domain transient signal when transforming into the frequency domain using inverse Fourier sine or cosine transforms.

The time domain impulse response function relates the polarization at time t to the electric field in the past:

$$P(t)=\epsilon_0\int_0^\infty \chi(\tau)E(t-\tau)d\tau. \tag{A1}$$

$\chi(t)$ is real and, by causality, $\chi(t)=0$ for $t<0$. The susceptibility is defined by inverse Fourier transformation of the impulse response,

$$\hat{\chi}(\omega)=\int_0^\infty \chi(t)\exp(i\omega t)dt. \tag{A2}$$

The susceptibility is complex-valued $\hat{\chi}(\omega)=\chi'(\omega)+i\chi''(\omega)$, and the imaginary part alone determines the dissipation of field energy into the medium. The Kramers–Kronig relations[118] between the absorptive susceptibility $\chi''(\omega)$ and the dispersive susceptibility $\chi'(\omega)$ are

$$\chi'(\omega)=\frac{1}{\pi}\mathrm{PV}\int_{-\infty}^{\infty}\frac{\chi''(\omega')}{\omega'-\omega}d\omega,$$

and

$$\chi''(\omega)=-\frac{1}{\pi}\mathrm{PV}\int_{-\infty}^{\infty}\frac{\chi'(\omega')}{\omega'-\omega}d\omega, \tag{A3}$$

where PV represents the Cauchy principal value.[155] For *any* even function of frequency $f(\omega)$ (such as $f(\omega)=\omega\chi''(\omega)|e(\omega)|^2$ appearing in Eq. (9) or $\chi'(\omega)$ in Eq. (A3), one can obtain the result

$$\int_0^\infty\left[\frac{2}{\pi}\int_0^\infty f(\omega)\cos(\omega t)d\omega\right]\sin(\omega t)dt = -\frac{1}{\pi}\mathrm{PV}\int_{-\infty}^{\infty}\frac{f(\omega')}{\omega'-\omega}d\omega'. \tag{A4}$$

We now show how to obtain Eq. (A4). Using the even property of $f(\omega)$, the integral in parentheses on the left-hand side of Eq. (A4) can be extended to negative frequencies and written as a Fourier transform.

$$\frac{2}{\pi}\int_0^\infty f(\omega)\cos(\omega t)d\omega = 2\left(\frac{1}{2\pi}\int_{-\infty}^{\infty}f(\omega)\exp(-i\omega t)d\omega\right) = 2\,f(t). \tag{A5}$$

We abbreviate the integral in parentheses in Eq. (A5) as $f(t)$ since it is the Fourier transform of $f(\omega)$. $f(t)$ is a real and even function of time (e.g., $\phi_0=0$ phase-locked pulse pair absorption signal). We now take the inverse Fourier sine transform of $2\,f(t)$ over the domain $(0,+\infty)$ as in Eq. (A4).

$$\int_0^\infty\left[\frac{2}{\pi}\int_0^\infty f(\omega)\cos(\omega t)d\omega\right]\sin(\omega t)dt = 2\int_0^\infty f(t)\sin(\omega t)dt. \tag{A6}$$

Taking the inverse sine transform of an even function, which has no sinusoidal Fourier components, seems to be a suspect step.[156,157] The steps below use the true even symmetry of $f(t)$; the implicit assumption that $f(t)$ has sinusoidal components in the inverse sine transform will not be used again. The next step is to use the sign function (defined in Sec. II) to rewrite the inverse sine transform in Eq. (A6) so that it can be extended over the entire real axis as an inverse Fourier transform

$$2\int_0^\infty f(t)\sin(\omega t)dt = 2\int_0^\infty[-if(t)][i\sin(\omega t)]dt = 2\int_0^\infty[-i\,\mathrm{sign}(t)\times f(t)][i\sin(\omega t)]dt. \tag{A7}$$

Since $f(t)$ is even and sing(t) is odd, the product $[\mathrm{sign}(t)\times f(t)]$ is odd, and the inverse sine transform can be converted to an inverse Fourier transform with limits $(-\infty,+\infty)$,

$$2\int_0^\infty[-i\,\mathrm{sign}(t)\times f(t)][i\sin(\omega t)]dt = \int_{-\infty}^{\infty}[-i\,\mathrm{sign}(t)\times f(t)]\exp(i\omega t)dt. \tag{A8}$$

The inverse Fourier transform of the product on the right-hand side of Eq. (A8) can be simplified along the lines of the convolution theorem (this has been used to define the Hilbert transform).[158] By using Eqs. (A6)–(A7) and substituting

$$\mathrm{PV}\int_{-\infty}^{\infty}\frac{1}{\pi\omega'}\exp(-i\omega' t)d\omega' = \begin{pmatrix} -i & (t>0)\\ 0 & (t=0)\\ +i & (t<0)\end{pmatrix} = -i\,\mathrm{sign}(t), \tag{A9}$$

into the right-hand side of Eq. (A8), we obtain

$$\int_0^\infty\left[\frac{2}{\pi}\int_0^\infty f(\omega)\cos(\omega t)d\omega\right]\sin(\omega t)dt = 2\int_{-\infty}^{\infty}f(t)\cdot\left(\frac{1}{2\pi}\mathrm{PV}\int_{-\infty}^{\infty}\frac{1}{\omega'}\exp(-i\omega' t)d\omega'\right)\times\exp(i\omega t)dt. \tag{A10}$$

First, the order of time and frequency integrations is interchanged,

$$=\frac{1}{\pi}\mathrm{PV}\int_{-\infty}^{\infty}\frac{1}{\omega'}\int_{-\infty}^{\infty}f(t)\exp[i(\omega-\omega')t]dtd\omega',$$

then the time domain inverse Fourier transform of $f(t)$ is evaluated,

$$=\frac{1}{\pi}\mathrm{PV}\int_{-\infty}^{\infty}\frac{1}{\omega'}f(\omega-\omega')d\omega',$$

and the resulting integral is rearranged by substitution to yield a Kramers–Kronig inversion

$$=-\frac{1}{\pi}\mathrm{PV}\int_{-\infty}^{\infty}\frac{f(\omega')}{\omega'-\omega}d\omega' = -\mathrm{KK}[f(\omega)]. \tag{A11}$$

Eq. (A11) has exactly the same form as the second Kramers–Kronig relation in Eq. (A3). An inverse sine transformation of even time domain data over the range $(0,\infty)$ is exactly equivalent to a Kramers–Kronig inversion. Similarly, one can start with any odd function $g(\omega)$, [such as $g(\omega)=\omega\chi''(\omega)\cdot|e(\omega)|^2\mathrm{sign}(\omega)$ in Eq. (9c) or $\chi''(\omega)$ in Eq. (A3)] and obtain

$$\int_0^\infty\left[\frac{2}{\pi}\int_0^\infty g(\omega)\sin(\omega t)d\omega\right]\cos(\omega t)dt = \frac{1}{\pi}\mathrm{PV}\int_{-\infty}^{\infty}\frac{g(\omega')}{\omega'-\omega}d\omega' = \mathrm{KK}[g(\omega)], \tag{A12}$$

which matches the first Kramers–Kronig relation in Eq. (A3). An inverse cosine transformation of odd time domain data over the range $(0,\infty)$ is exactly equivalent to a Kramers–Kronig inversion. As in the Kramers–Kronig relations, the sign of the principal value integral in Eqs. (A11) and (A12) is determined by the even $[f(\omega)$ or $\chi'(\omega)]$ or odd $[g(\omega)$ or $\chi''(\omega)]$ symmetry of the function being transformed. Similar relations have been used for rapid Kramers–Kronig inversion by several workers.[157,159–161]

When the phase difference between phase-locked pulses is 0, Eq. (9b) shows that the interference signal is proportional to the cosine transform of the product $\omega\chi''(\omega)\cdot|e(\omega)|^2/|\omega|$ and is an even function of time. Taking the inverse sine transform of a Nyquist sampled $\phi_0=0$ phase-locked pulse pair signal [as in Eq. (3.24) of Ref. 13] is thus

equivalent to Kramers–Kronig inversion of the experimentally measured product $\omega\chi''(\omega)\cdot|e(\omega)|^2/|\omega|$. Similarly, Eq. (9c) shows the $\pi/2$ phase-locked pulse pair signal *appears* to be the sine transform of the product $\omega\chi''(\omega)\cdot|e(\omega)|^2/|\omega|$, and is an odd function of time. From Eq. (A12), inverse cosine transformation of the $\pi/2$ phase shifted signal is equivalent to a Kramers–Kronig inversion of the limited bandwidth product $\omega\chi''(\omega)\cdot|e(\omega)|^2/|\omega|$.

In principle, the Kramers–Kronig relation applies over the entire real axis. In practice, the dispersive susceptibility is often significant in transparency regions where the absorptive susceptibility is near zero (e.g., the refractive index of glass in the visible). An inverse cosine transform projects the transient onto cosinusoidal components, while an inverse sine transform projects the transient onto sinusoidal components, regardless of which components are present in the transient.[155] Taking an inverse cosine transformation of even time domain data (or an inverse sine transform of odd time domain data) recovers the experimentally measured observable in the frequency domain. However, a sine transform of even time domain data does not resemble the measured frequency domain observable because it projects the time domain signal onto oscillatory functions with opposite absorptive/dispersive character (cosinusoidal excitation produces cosinusoidal absorptive and sinusoidal dispersive components in a free induction decay). Because taking the sine transform of even time domain data (or the cosine transform of odd time domain data) is equivalent to a Kramers–Kronig inversion of finite frequency bandwidth data, the results of such a transformation *deceptively resemble* a measurement of dispersion when the experiment measures only absorption. In some ways, the ability of an experiment to recover absorption and dispersion spectra which disagree with a Kramers–Kronig inversion of each other (due to the effect of absorption bands outside the range of the pulse spectra on the refractive index)[115] is a useful test for true measurement of the dispersive susceptibility.

[1] D. J. Tannor, R. Kosloff, and S. A. Rice, J. Chem. Phys. **85**, 5805 (1986).
[2] D. J. Tannor and S. A. Rice, Adv. Chem. Phys. **70**, 441 (1988).
[3] P. Brumer and M. Shapiro, Acc. Chem. Res. **22**, 407 (1989).
[4] W. S. Warren, H. Rabitz, and M. Dahleh, Science **259**, 1581 (1993).
[5] M. Shapiro and P. Brumer, Int. Rev. Phys. Chem. **13**, 187 (1994).
[6] R. J. Gordon and S. A. Rice, Annu. Rev. Phys. Chem. **48**, 601 (1997).
[7] L. Zhu, K. Suto, J. A. Fiss, R. Wada, T. Seideman, and R. J. Gordon, Phys. Rev. Lett. **79**, 4108 (1997).
[8] R. N. Zare, J. Chem. Phys. **279**, 1875 (1998).
[9] W. S. Warren and A. H. Zewail, J. Chem. Phys. **78**, 2279 (1983).
[10] F. Spano, M. Haner, and W. S. Warren, Chem. Phys. Lett. **135**, 97 (1987).
[11] N. F. Scherer, A. J. Ruggiero, M. Du, and G. R. Fleming, J. Chem. Phys. **93**, 856 (1990).
[12] N. F. Scherer, R. J. Carlson, A. Matro, M. Du, A. J. Ruggiero, V. Romero-Rochin, J. A. Cina, G. R. Fleming, and S. A. Rice, J. Chem. Phys. **95**, 1487 (1991).
[13] N. F. Scherer, A. Matro, L. D. Ziegler, M. Du, R. J. Carlson, J. A. Cina, and G. R. Fleming, J. Chem. Phys. **96**, 4180 (1992).
[14] M. Cho, N. F. Scherer, G. R. Fleming, and S. Mukamel, J. Chem. Phys. **96**, 5618 (1992).
[15] L. D. Ziegler and N. F. Scherer, J. Chem. Phys. **7**, 4704 (1992).
[16] W. P. de Boeij, M. S. Pshenichnikov, and D. A. Wiersma, Chem. Phys. Lett. **238**, 1 (1995).
[17] W. P. de Boeij, M. S. Pshenichnikov, and D. A. Wiersma, Chem. Phys. Lett. **247**, 264 (1995).
[18] W. P. de Boeij, M. S. Pshenichnikov, and D. A. Wiersma, Chem. Phys. **233**, 287 (1998).
[19] C. J. Kennedy, Appl. Opt. **15**, 2623 (1976).
[20] E. Hecht, *Optics*, 2nd ed. (Addison-Wesley, Reading, MA, 1990).
[21] F. A. Jenkins and H. E. White, *Fundamentals of Optics*, 4th ed. (McGraw-Hill, New York, 1976).
[22] M. Born and E. Wolf, *Principles of Optics*, 2nd ed. (Pergamon, New York, 1964).
[23] N. A. Ramsey, Rev. Mod. Phys. **62**, 541 (1990).
[24] J. K. M. Sanders and B. K. Hunter, *Modern NMR Spectroscopy: A Guide for Chemists* (Oxford University Press, Oxford, 1987).
[25] R. R. Ernst, G. Bodenhausen, and A. Wokaun, *Principles of Nuclear Magnetic Resonance in One and Two Dimensions* (Oxford University Press, Oxford, 1987).
[26] C. Leichtle, W. P. Schleich, I. S. Averbukh, and M. Shapiro, J. Chem. Phys. **108**, 6057 (1998).
[27] S. Mukamel, Annu. Rev. Phys. Chem. **41**, 647 (1990).
[28] S. Mukamel, *Principles of Nonlinear Optical Spectroscopy* (Oxford University Press, New York, 1995).
[29] X.-P. Jiang and P. Brumer, J. Chem. Phys. **94**, 5833 (1991).
[30] X.-P. Jiang, M. Shapiro, and P. Brumer, J. Chem. Phys. **104**, 607 (1996).
[31] H. Tang, R. Kosloff, and S. A. Rice, J. Chem. Phys. **104**, 5457 (1996).
[32] D. G. Abrashkevich, M. Shapiro, and P. Brumer, J. Chem. Phys. **108**, 3585 (1998).
[33] A. Brown and W. J. Meath, J. Chem. Phys. **109**, 9351 (1998).
[34] L. Xu, C. Spielmann, A. Poppe, T. Brabec, F. Krausz, and T. W. Hänsch, Opt. Lett. **21**, 2008 (1996).
[35] The magnitude and sign of the momentum impulse imparted to a free charge by a short optical pulse should depend on the absolute phase of the pulse.
[36] W. H. Press, B. P. Flannery, S. A. Teukolsky, and W. T. Vettering, *Numerical Recipes: The Art of Scientific Computing* (Cambridge University Press, New York, 1986).
[37] R. J. Bell, *Introductory Fourier Transform Spectroscopy* (Academic, New York, 1972).
[38] A. G. Marshall and F. R. Verdun, *Fourier Transforms in NMR, Optical, and Mass Spectrometry: a User's Handbook* (Elsevier, New York, 1990).
[39] D. S. Chemla, J.-Y. Bigot, M.-A. Mycek, S. Weiss, and W. Schäfer, Phys. Rev. B **50**, 8439 (1994).
[40] J.-P. Likforman, M. Joffre, and V. Thierry-Mieg, Opt. Lett. **22**, 1104 (1997).
[41] M. F. Emde, W. P. de Boeij, M. S. Pshenichnikov, and D. A. Wiersma, Opt. Lett. **22**, 1338 (1997).
[42] S. M. Gallagher, A. W. Albrecht, J. D. Hybl, B. L. Landin, B. Rajaram, and D. M. Jonas, J. Opt. Soc. Am. B **15**, 2338 (1998).
[43] J. D. Hybl, A. W. Albrecht, S. M. Gallagher Faeder, and D. M. Jonas, Chem. Phys. Lett. **297**, 307 (1998).
[44] A. M. Weiner, S. De Silvestri, and E. P. Ippen, J. Opt. Soc. Am. B **2**, 654 (1985).
[45] W. M. Zhang, V. Chernyak, and S. Mukamel, J. Chem. Phys. **110**, 5011 (1999).
[46] Y. R. Shen, *The Principles of Nonlinear Optics* (Wiley-Interscience, New York, 1984).
[47] The envelope phase of the above quasimonochromatic approximation to a pulse thus varies as the pulse propagates through the sample. At a single point in space, the quasimonochromatic field given above also has a constant carrier wave phase as the delay is varied (hence an envelope phase-shift).
[48] M. Schubert and B. Wilhelmi, *Nonlinear Optics and Quantum Electronics* (Wiley-Interscience, New York, 1986).
[49] I. D. Abella, N. A. Kurnit, and S. R. Hartmann, Phys. Rev. **141**, 391 (1966).
[50] T. W. Mossberg, R. Kachru, S. R. Hartmann, and A. M. Flusberg, Phys. Rev. A **20**, 1976 (1979).
[51] Y.-X. Yan, E. B. Gamble, and K. A. Nelson, J. Chem. Phys. **83**, 5391 (1985).
[52] K. A. Nelson and E. P. Ippen, Adv. Chem. Phys. **75**, 1 (1989).
[53] T. Brabec and F. Krausz, Phys. Rev. Lett. **78**, 3282 (1997).
[54] J. A. Stratton, *Electromagnetic Theory* (McGraw-Hill, New York, 1941).
[55] F. Reynaud, F. Salin, and A. Barthelmy, Opt. Lett. **14**, 275 (1989).
[56] E. Tokunaga, A. Terasaki, and T. Kobayashi, Opt. Lett. **17**, 1131 (1992).
[57] E. Tokunaga, A. Terasaki, and T. Kobayashi, J. Opt. Soc. Am. B **12**, 753 (1995).

[58] L. Lepetit, G. Chériaux, and M. Joffre, J. Opt. Soc. Am. B **12**, 2467 (1995).
[59] D. N. Fittinghoff, J. L. Bowie, J. N. Sweetser, R. T. Jennings, M. A. Krumbügel, K. W. DeLong, R. Trebino, and I. A. Walmsley, Opt. Lett. **21**, 884 (1996).
[60] D. N. Fittinghoff, J. L. Bowie, J. N. Sweetser, R. T. Jennings, M. A. Krumbügel, K. W. DeLong, R. Trebino, and I. A. Walmsley, Opt. Lett. **21**, 1313 (1996).
[61] S. Mukamel and R. F. Loring, J. Opt. Soc. Am. B **3**, 595 (1986).
[62] Y. J. Yan and S. Mukamel, J. Chem. Phys. **89**, 5160 (1988).
[63] Y. J. Yan and S. Mukamel, J. Chem. Phys. **94**, 179 (1991).
[64] Y. Tanimura and S. Mukamel, J. Chem. Phys. **99**, 9496 (1993).
[65] V. Chernyak, W. M. Zhang, and S. Mukamel, J. Chem. Phys. **109**, 9587 (1998).
[66] S. M. Gallagher Faeder and D. M. Jonas, J. Phys. Chem. A (in press).
[67] S. M. Gallagher Faeder, Ph.D. thesis, University of Colorado, 1999.
[68] L. Lepetit and M. Joffre, Opt. Lett. **21**, 564 (1996).
[69] A. Tokmakoff, M. J. Lang, D. S. Larsen, G. R. Fleming, V. Chernyak, and S. Mukamel, Phys. Rev. Lett. **79**, 2702 (1997).
[70] I. Levy, M. Shapiro, and P. Brumer, J. Chem. Phys. **93**, 2493 (1990).
[71] K. Okumura and Y. Tanimura, Chem. Phys. Lett. **295**, 298 (1998).
[72] M. Takeda, Jpn. J. Opt. **13**, 55 (1984).
[73] C. Dorrer, J. Opt. Soc. Am. B **16**, 1160 (1999).
[74] D. A. Wiersma and K. Duppen, Science **237**, 1147 (1987).
[75] Y. Nagasawa, J.-Y. Yu, and G. R. Fleming, J. Chem. Phys. **109**, 6175 (1998).
[76] M. Kujawinska, in *Interferogram Analysis: Digital Fringe Pattern Measurement Techniques*, edited by D. W. Robinson and G. T. Reid (Institute of Physics, Philadelphia, 1993), pp. 141-193.
[77] *Selected Papers on Interference, Interferometry, and Interferometric Metrology*, edited by P. Hariharan and D. Malacara (SPIE Optical Engineering, Bellingham, WA, 1995), Vol. MS 110.
[78] This result can be derived by inserting a phase-shift ϕ in the derivation of the electric field diffracted by a sound wave given in Ch. 12 of A. Yariv, *Optical Electronics in Modern Communications*, 5th ed. (Oxford University Press, New York, 1997). This result also holds for absorption coefficient gratings.
[79] H. Petek and S. Ogawa, Prog. Surf. Sci. **56**, 239 (1997).
[80] W. Nessler, S. Ogawa, H. Nagano, H. Petek, J. Shimoyama, Y. Nakayama, and K. Kishio, J. Electron Spectrosc. Relat. Phenom. **88-91**, 495 (1998).
[81] S. Ogawa, H. Nagano, H. Petek, and A. P. Heberle, Phys. Rev. Lett. **78**, 1339 (1997).
[82] A. P. Heberle, J. J. Baumberg, and K. Köhler, Phys. Rev. Lett. **75**, 2598 (1995).
[83] H. Petek, A. P. Heberle, W. Nessler, S. Kubota, S. Matsunami, N. Moriya, and S. Ogawa, Phys. Rev. Lett. **79**, 4649 (1997).
[84] H. Kawashima, M. M. Wefers, and K. A. Nelson, Annu. Rev. Phys. Chem. **46**, 627 (1995).
[85] N. H. Bonadeo, J. Erland, D. Gammon, D. Park, D. S. Katzer, and D. G. Steel, Science **282**, 1473 (1998).
[86] D. Marcuse, *Principles of Quantum Electronics* (Academic, New York, 1980).
[87] K. Creath, in *Interferogram Analysis: Digital Fringe Pattern Measurement Techniques*, edited by D. W. Robinson and G. T. Reid (Institute of Physics, Philadelphia, 1993), pp. 95-140.
[88] V. Nagarajan, E. Johnson, J. C. Williams, and W. W. Parson, J. Phys. Chem. B **103**, 2297 (1999).
[89] T. Radhakrishan, Proc.-Indian Acad. Sci., Sect. A **33**, 22 (1951).
[90] *Properties of Optical and Laser-Related Materials: a Handbook*, edited by D. N. Nikogosyan (Wiley, Chichester, 1997).
[91] A. A. Michelson, *Studies in Optics* (University of Chicago Press, Chicago, 1927).
[92] G. D. Goodno, G. Dadusc, and R. J. Dwayne Miller, J. Opt. Soc. Am. B **15**, 1791 (1998).
[93] R. R. Jones, C. S. Raman, D. W. Schumacher, and P. H. Bucksbaum, Phys. Rev. Lett. **71**, 2575 (1993).
[94] A. E. Siegman, *Lasers* (University Science Books, Mill Valley, CA, 1986).
[95] C. Spielmann, L. Xu, and F. Krausz, Appl. Opt. **36**, 2523 (1997).
[96] M. S. Pshenichnikov, W. P. de Boeij, and D. A. Wiersma, Opt. Lett. **19**, 572 (1994).
[97] M. Wefers and K. A. Nelson, Opt. Lett. **18**, 2032 (1993).
[98] W. Yang, D. Keusters, D. Goswami, and W. S. Warren, Opt. Lett. **23**, 1843 (1998).
[99] J. X. Tull, M. A. Dugan, and W. S. Warren, Adv. Magn. Opt. Reson. **20**, 1 (1997).
[100] M. M. Salour and C. Cohen-Tannoudji, Phys. Rev. Lett. **38**, 757 (1977).
[101] M. M. Salour, Rev. Mod. Phys. **50**, 667 (1978).
[102] J. C. Bergquist, S. A. Lee, and J. L. Hall, Phys. Rev. Lett. **38**, 159 (1977).
[103] J. T. Fourkas, W. L. Wilson, G. Wäckerle, A. E. Frost, and M. D. Fayer, J. Opt. Soc. Am. B **6**, 1905 (1989).
[104] Random optical path length variations lead to random delay variations and not random variation of the constant term in the spectral phase which is called the phase of a pulse here.
[105] This difference makes the term $(\omega_L t_d + \phi)$ in the argument of the cosine in Eq. (4.35) of Ref. 12 and Eq. (3.6) of Ref. 13 identically zero (mod 2π) in the phase-locked pulse pair experiments.
[106] E. J. Heller, in *Ultrafast Phenomena VII*, edited by C. B. Harris, E. P. Ippen, G. A. Mourou, and A. H. Zewail (Springer-Verlag, Berlin, 1990).
[107] R. Bavli, V. Engel, and H. Metiu, J. Chem. Phys. **96**, 2600 (1992).
[108] G. M. Lankhuijzen and L. D. Noordam, Phys. Rev. A **52**, 2016 (1995).
[109] R. R. Jones, D. W. Schumacher, T. F. Gallagher, and P. H. Bucksbaum, J. Phys. B **28**, L405 (1995).
[110] V. Blanchet, M. A. Bouchène, and B. Girard, J. Chem. Phys. **108**, 4862 (1998).
[111] A. G. Marshall, Chemom. Intell. Lab. Syst. **3**, 261 (1988).
[112] E. Bartholdi and R. R. Ernst, J. Magn. Reson. **11**, 9 (1973).
[113] L. I. Schiff, *Quantum Mechanics*, 3rd ed. (McGraw-Hill, New York, 1968).
[114] E. C. Kemble, *The Fundamental Principles of Quantum Mechanics*, 1st ed. (McGraw-Hill, New York, 1937).
[115] M. Beck, I. A. Walmsley, and J. D. Kafka, IEEE J. Quantum Electron. **27**, 2074 (1991).
[116] L. D. Landau, E. M. Lifschitz, and L. P. Pitaevskii, *Electrodynamics of Continuous Media*, 2nd ed. (Pergamon, New York, 1984).
[117] J. D. Jackson, *Classical Electrodynamics*, 2nd ed. (Wiley, New York, 1975).
[118] A. Yariv, *Optical Electronics in Modern Communications*, 5th ed. (Oxford University Press, New York, 1997).
[119] M. L. Forman, W. H. Steel, and G. A. Vanasse, J. Opt. Soc. Am. **56**, 59 (1966).
[120] J. A. Cina (personal communication, 1999).
[121] V. Volterra, *Theory of Functionals* (Blackie, London, 1930).
[122] P. N. Butcher and D. Cotter, *The Elements of Nonlinear Optics* (Cambridge University Press, New York, 1991).
[123] C. P. Slichter, *Principles of Magnetic Resonance*, 3rd ed. (Springer, New York, 1990).
[124] Y. R. Shen and N. Bloembergen, Phys. Rev. A **137**, 1787 (1965).
[125] D. Lee and A. C. Albrecht, Adv. Chem. Phys. **83**, 43 (1993).
[126] Y. Tanimura and S. Mukamel, Phys. Rev. E **47**, 118 (1993).
[127] R. Trebino and D. J. Kane, J. Opt. Soc. Am. A **10**, 1101 (1993).
[128] J. Paye, IEEE J. Quantum Electron. **30**, 2693 (1994).
[129] K. W. DeLong and R. Trebino, J. Opt. Soc. Am. A **11**, 2429 (1994).
[130] K. W. DeLong, R. Trebino, J. Hunter, and W. E. White, J. Opt. Soc. Am. B **11**, 2206 (1994).
[131] J. T. Fourkas, L. Dhar, K. A. Nelson, and R. Trebino, J. Opt. Soc. Am. B **12**, 155 (1995).
[132] K. W. DeLong, D. N. Fittinghoff, and R. Trebino, IEEE J. Quantum Electron. **32**, 1253 (1996).
[133] G. Taft, A. Rundquist, M. M. Murnane, I. P. Christov, H. C. Kapteyn, K. W. DeLong, D. N. Fittinghoff, M. A. Krumbügel, J. N. Sweetser, and R. Trebino, IEEE J. Sel. Top. Quantum Electron. **2**, 575 (1996).
[134] R. Trebino, K. W. DeLong, D. N. Fittinghoff, J. N. Sweetser, M. A. Krumbügel, B. A. Richman, and D. J. Kane, Rev. Sci. Instrum. **68**, 3277 (1997).
[135] Some discussions of FROG do not distinguish electric field from complex envelope. References 127 and 132–134 use the word ''field'' (often with complex conjugate notation) for complex envelope, while Refs. 128 through 131 explicitly use the complex envelope to calculate FROG signals. The equations for transient grating and self diffraction FROG signals in Ref. 134 are equal to the nonlinear polarization given by Eq. (13) when the response is instantaneous (i.e., the response function is a product of delta functions). Extensions of Eq. (14) may be useful for inverting interferometric FROG traces.
[136] T. Joo, Y. Jia, J.-Y. Yu, M. J. Lang, and G. R. Fleming, J. Chem. Phys. **104**, 6089 (1996).

[137] W. P. de Boeij, M. S. Pshenichnikov, K. Duppen, and D. A. Wiersma, Chem. Phys. Lett. **224**, 243 (1994).
[138] A. M. Weiner, IEEE J. Quantum Electron. **QE-19**, 1276 (1983).
[139] Y. R. Shen, Phys. Rev. B **9**, 622 (1974).
[140] L. D. Ziegler, Acc. Chem. Res. **27**, 1 (1994).
[141] As for linear experiments with phase-locked pulse pairs, a time domain analysis leads to the same conclusion if each member of both pulse pairs is treated symmetrically (e.g., pulse *c* should be included once as an excitation field in calculating the nonlinear polarization with pulse *d* as heterodyne field, and once as a heterodyne field when pulse *d* acts as a nonlinear excitation field).
[142] D. W. Phillion, D. J. Kuizenga, and A. E. Siegman, Appl. Phys. Lett. **27**, 85 (1975).
[143] K. A. Nelson, R. Casalegno, R. J. Dwayne Miller, and M. D. Fayer, J. Chem. Phys. **77**, 1144 (1982).
[144] M. D. Levenson and G. L. Eesley, Appl. Phys. **19**, 1 (1979).
[145] D. S. Alavi, R. S. Hartman, and D. H. Waldeck, J. Chem. Phys. **92**, 4055 (1990).
[146] P. Brumer and M. Shapiro, Chem. Phys. **139**, 221 (1989).
[147] J. Cao and K. R. Wilson, J. Chem. Phys. **107**, 1441 (1997).
[148] J. L. Herek, A. Materny, and A. H. Zewail, Chem. Phys. Lett. **228**, 15 (1994).
[149] C. J. Bardeen, J. Che, K. R. Wilson, V. Yakovlev, P. Cong, J. Krause, and M. Messina, J. Phys. Chem. A **101**, 3815 (1997).
[150] R. Uberna, M. Khalil, R. M. Williams, J. M. Papanikolas, and S. R. Leone, J. Chem. Phys. **108**, 9259 (1998).
[151] M. Shapiro and P. Brumer, J. Chem. Soc., Faraday Trans. **93**, 1263 (1997).
[152] J. A. Fiss, L. Zhu, and R. J. Gordon, Phys. Rev. Lett. **82**, 65 (1999).
[153] Dephasing can prevent molecules from seeing the global phase relationship between long or widely separated pulses. Harmonics have a locally periodic phase relationship which repeats every period of the lowest harmonic so that the global phase relationship is apparent on a very short time scale.
[154] E. C. Titchmarsh, *Introduction to the Theory of Fourier Integrals*, 2nd ed. (Oxford University Press, London, 1959).
[155] G. Arfken, *Mathematical Methods for Physicists* (Academic, New York, 1985).
[156] For a causal impulse response [e.g., $\chi(t)$ in Eq. (A2)], the unique even and odd extensions of that response are equal for positive times and may be substituted one for the other in truncated Fourier sine and cosine transforms to formally derive the Kramers–Kronig relations based only on linear response and causality (see Ref. 157). Subtleties associated with poles of $\chi(\omega)$ in the complex analytic derivation of the Kramers–Kronig relations are hidden in the impulse response at $t=0$.
[157] C. W. Peterson and B. W. Knight, J. Opt. Soc. Am. **63**, 1238 (1973).
[158] H. Dym and H. P. McKean, *Fourier Series and Integrals* (Academic, New York, 1972).
[159] M. G. Sceats and G. C. Morris, Phys. Status Solidi A **14**, 643 (1972).
[160] J. A. Bardwell and M. J. Dignam, J. Chem. Phys. **83**, 5468 (1985).
[161] C. P. Williams and A. G. Marshall, Anal. Chem. **64**, 916 (1992).